JHEP

Published by Institute of Physics Publishing for SISSA

Received: *November 3, 2005*
Accepted: *January 12, 2006*
Published: *January 25, 2006*

The phase structure of low dimensional large N gauge theories on tori

Ofer Aharony,[a] **Joe Marsano,**[bc] **Shiraz Minwalla,**[cb] **Kyriakos Papadodimas,**[bc] **Mark Van Raamsdonk**[d] **and Toby Wiseman**[b]

[a] *Department of Particle Physics, Weizmann Institute of Science Rehovot 76100, Israel*
[b] *Jefferson Physical Laboratory, Harvard University Cambridge, MA 02138, U.S.A.*
[c] *Department of Theoretical Physics, Tata Institute of Fundamental Research Homi Bhabha Rd, Mumbai 400005, India*
[d] *Department of Physics and Astronomy, University of British Columbia Vancouver, BC, V6T 1Z1, Canada*
E-mail: ofer.aharony@weizmann.ac.il, marsano@fas.harvard.edu, minwalla@theory.tifr.res.in, papadod@fas.harvard.edu, mav@physics.ubc.ca, wiseman@sakurai.physics.harvard.edu

Abstract: In this paper we continue our study of the thermodynamics of large N gauge theories on compact spaces. We consider toroidal compactifications of pure SU(N) Yang-Mills theories and of maximally supersymmetric Yang-Mills theories dimensionally reduced to $0+1$ or $1+1$ dimensions, and generalizations of such theories where the adjoint fields are massive. We describe the phase structure of these theories as a function of the gauge coupling, the geometry of the compact space and the mass parameters. In particular, we study the behavior of order parameters associated with the holonomy of the gauge field around the cycles of the torus. Our methods combine analytic analysis, numerical Monte Carlo simulations, and (in the maximally supersymmetric case) information from the dual gravitational theories.

Keywords: 1/N Expansion, Field Theories in Lower Dimensions, AdS-CFT Correspondence.

JHEP01(2006)140

Contents

JHEP01(2006)140

1. Introduction

In this paper we study one and two dimensional Euclidean SU(N) Yang-Mills theories compactified on a circle and on a torus, respectively. This is relevant in particular for studying these theories at finite temperature. In the 't Hooft large N limit, we determine the phase diagrams of these theories as a function of masses (of adjoint matter fields), coupling constants and compactification parameters. The systems we study exhibit rich dynamics; in particular, they undergo sharp large N phase transitions upon varying parameters. These phase transitions are associated with the spontaneous breakdown of the $\mathbb{Z}_N$ symmetry $W \to e^{\frac{2\pi i}{N}} W$, where W is the holonomy along a non-contractible cycle of the compactification manifold.

Our analysis employs different techniques in different regimes of parameter space. When all matter fields are very massive compared to the scale set by the gauge coupling (more precisely, when $m^{4-d} \gg \lambda$, where m is the mass scale of the matter fields, d is the dimension of space-time and $\lambda \equiv g_{YM}^2 N$ is the 't Hooft coupling), the gauge theories we study are weakly coupled[1], and may reliably be analyzed in perturbation theory. Already in this analytically tractable regime our systems undergo sharp phase transitions and display a rich phase structure. Outside this perturbative regime, the phase diagrams we study can be constrained by the requirement that they reproduce well known results in special limits. The strong coupling behavior of maximally supersymmetric Yang-Mills theories may be analyzed using generalizations of the AdS/CFT correspondence. Finally, it is sometimes practical to employ Monte Carlo simulations to supplement the information from our other techniques. Employing all these methods, we are able to present a reasonably complete picture of the phase diagram of the systems we study.

The investigations reported in this paper are similar in spirit to the recent study of Yang-Mills theory on $S^p \times S^1$ [1, 2]. It may be recalled that the phase transitions discovered in [1, 2] may be thought of as a weak coupling continuation of the gravitational Hawking-Page transition in $AdS_5 \times S^5$. At least some of the phase transitions we study in this paper also have gravitational analogues. For example, as we have already reported in the letter [3] (building on the work of [4 – 6]), the phase transition in maximally supersymmetric Yang-Mills theory on T^2 is holographically dual to a Gregory-Laflamme black hole/black string phase transition in type II string theory. See section 7 for other examples.

[1] Recall that the massless gauge field has no dynamical degrees of freedom.

JHEP01(2006)140

The structure of this paper is as follows. In section 2, we discuss various general properties of low dimensional gauge theories on tori, and in particular the order parameters that distinguish the various phases that appear. In section 3, we review the behavior of Yang-Mills theory dimensionally reduced to 0 dimensions; this is relevant to the small volume limit of the higher dimensional cases. In section 4, we use analytic and numerical techniques to map out the phase diagram of pure $p+1$-dimensional gauge theory dimensionally reduced to 0+1 dimensions, and its generalizations with masses for the adjoint scalars. In section 5, we study the thermodynamics of 1+1 dimensional Yang-Mills theory with massive or massless adjoint scalars on a spatial circle by studying the partition function of Euclidean two dimensional Yang-Mills theory on T^2. In the case where the scalars are very massive, we obtain a fairly complete picture of the rather rich phase structure through analytic analysis, leading to the phase diagrams in figures 14 and 15. In sections 6 and 7, we repeat the analysis of sections 4 and 5 for the maximally supersymmetric Yang-Mills theories in $0+1$ and $1+1$ dimensions, respectively. For these theories, knowledge of the dual gravitational theories provides additional information about the strong coupling behavior of the gauge theory. We find that the supersymmetric theories show rather different qualitative behavior from the non-supersymmetric theories; for the two dimensional case this behavior is summarized in the phase diagrams of figures 18 and 19.

2. Low dimensional Yang-Mills theory on tori: generalities

Massless vector fields have no propagating degrees of freedom in one and two dimensions. As a consequence, pure Yang-Mills theory in these dimensions is exactly solvable, and exhibits relatively tame dynamics. However, the same theory displays rich dynamical behavior when coupled to matter fields. In this paper we will study large N SU(N) Yang-Mills theories coupled to matter fields in the adjoint representation. We begin in this section with an overview of the properties of these theories.

2.1 Quantum mechanical gauge theories ($d = 1$)

Different SU(N) quantum mechanical gauge theories with adjoint scalar fields can behave in at least three qualitatively distinct ways in the IR. In some theories an attractive effective potential (at long range) between the eigenvalues of the scalar fields ensures that the vacuum state is normalizable, and that the spectrum is gapped. In other theories, the scalar potential has exactly flat directions and the spectrum is ungapped. In yet other theories the long-range scalar effective potential is repulsive; such theories lack a vacuum state.

Theories with a mass gap (see section 4 below for a detailed study of one class of examples) may be thought of as one dimensional analogues of confining theories in $d = 4$. In the 't Hooft large N limit with fixed $\lambda \equiv g_{YM}^2 N$ [7], the spectrum of such theories is expected to display a Hagedorn-like growth in the density of states, with a high energy density of states $\rho(E) \sim \exp(E/T_H)$ for energies which remain finite in the large N limit (see section 2 of [2] for a simple example). It follows that, upon heating, these theories undergo a 'deconfinement' phase transition at or below their effective Hagedorn temperature T_H. In

other words, the Euclidean partition function on S^1 undergoes a phase transition when the circumference of the compactification circle is larger than or equal to the inverse Hagedorn temperature. The free energy jumps from $\mathcal{O}(1)$ at low temperatures to $\mathcal{O}(N^2)$ at high temperatures (where the theory is weakly coupled), so $\lim_{N\to\infty} F(T)/N^2$ may be viewed as an order parameter for the deconfinement transition. As in four dimensions, the expectation value of the Polyakov loop $\langle \mathrm{tr}(P \exp(i \oint A_0)) \rangle$ in the Euclidean theory is another order parameter for this phase transition [2].

Theories of the second type (those with a well-defined vacuum but an ungapped spectrum — see section 6 below for a detailed study of an example) may be thought of as the analogues of conformal theories in 4 dimensions. We expect such theories to be 'deconfined' at all temperatures. If such theories undergo phase transitions as a function of temperature (this may or may not happen), the two phases are distinguished by an order parameter more sensitive than the expectation value of the Polyakov loop or $F(T)/N^2$, each of which is nonzero in both phases.

We will not consider theories that lack a vacuum state in this paper.

2.2 $d = 2$ gauge theories

We begin by considering $1+1$ dimensional large N SU(N) Yang-Mills theories, with purely adjoint matter content, on $\mathbb{R}\times$time. Our general expectations for the thermodynamics of such systems are analogous to those for quantum mechanical systems reviewed in the previous subsection. Gapped theories are expected to have a Hagedorn growth in their density of states for energies which remain finite in the large N limit (see [2, 8] for examples). These theories are expected to undergo a deconfining phase transition at or below the Hagedorn temperature. The free energy is expected to be of order $\mathcal{O}(N^2)$ (and the Polyakov loop nonzero) at high temperatures, while the free energy is expected to be $\mathcal{O}(1)$ (and the Polyakov loop vanishes) at low temperatures. On the other hand the free energy in ungapped theories is expected to be $\mathcal{O}(N^2)$ (and the Polyakov loop expected to be nonzero) at all temperatures [3].

However, field theories in $d = 2$ have additional structure absent in $d = 1$. It is possible, and rather natural, to study the thermodynamics of such theories compactified on a spatial circle. In Euclidean space this thermodynamics is described by the partition function of the corresponding Yang-Mills theory on a T^2. This opens the possibility for a much richer phase structure in these models, as we explain in the rest of this subsection.

Recall that we are interested in SU(N) theories which only have fields in the adjoint representation. For such theories, the gauge group is really $\mathrm{SU}(N)/\mathbb{Z}_N$, since the gauge transformations in the $\mathbb{Z}_N$ center of the gauge group act trivially. Whenever such a theory

[2] The Polyakov loop vanishes at large circle radius but is non-zero at small radius (there is a subtlety in this statement; see footnote 5 below). Intuitively, the Polyakov loop vanishes at low temperatures in a theory with a mass gap because only an infinite number of adjoint photons can effectively screen a fundamental charge; the mass gap ensures that such a configuration has infinite energy. See section 5.7 of [2] for a more careful and detailed discussion.

[3] This is true generically, but it is not true in some supersymmetric examples in which the low temperature free energy is of order N.

is compactified on a torus, it possesses a $(\mathbb{Z}_N)_0 \times (\mathbb{Z}_N)_1$ global symmetry. This global symmetry is generated by gauge transformations G that are not periodic on the torus but instead obey $G(x^\mu + pe_0 + qe_1) = \alpha^p \beta^q G(x^\mu)$, where e_0 and e_1 are the fundamental cycles of the torus (along the 0 and 1 directions) and α and β are both gauge transformations in the center $\mathbb{Z}_N$. All local gauge-invariant operators are uncharged under this global symmetry, but fundamental Wilson lines that wrap around a (p, q) cycle before closing carry charge (p, q). Thus, non-zero expectation values for such Wilson loops break this global symmetry. In particular, an expectation value for the Wilson loop W_μ [4] spontaneously breaks the $(\mathbb{Z}_N)_\mu$ symmetry[5], where $\mu = 0, 1$.

As we will see later in this paper, in the decompactification limit $R_1 \to \infty$ the symmetry $(\mathbb{Z}_N)_1$ is never broken so W_1 always vanishes. The Polyakov loop W_0 is the sole order parameter for the system in this limit, making contact with the discussion at the beginning of this subsection. At finite R_1, W_0 and W_1 are both nontrivial order parameters, allowing for intricate two dimensional phase diagrams with the four possible phases separated by phase transition lines. Of course, such a phase diagram in a system that is ungapped in the decompactification ($R_1 \to \infty$) limit (see section 7 for an example) has qualitative differences from its counterpart in a theory that is gapped in the same limit (see section 5 for examples).

In the large N limit, instead of just considering the Wilson loop W_μ in the fundamental representation, it is often useful to study the full holonomy matrix $U_\mu(\vec{x}) = Pe^{i \oint A_\mu}$, which is a unitary matrix whose trace (in some representation) gives the Wilson loop (in that representation). The set of eigenvalues of this matrix (which live on the unit circle) is gauge-invariant, and in the large N limit their distribution along the unit circle is some continuous function. The $(\mathbb{Z}_N)_\mu$ global symmetry described above shifts the phases of all the eigenvalues of U_μ by an angle of $2\pi/N$. In the $\mathbb{Z}_N$-symmetric phase the large N eigenvalue distribution is constant, while otherwise it is generally maximized at some particular value, spontaneously breaking the $\mathbb{Z}_N$ symmetry. Detailed analysis of the eigenvalue distributions sometimes permits a sharp distinction between two phases with the same symmetry breaking pattern, allowing for the possibility of even more intricate phase diagrams (interpolating between a larger number of phases) than those described above.

2.3 On dimensional reduction

One of the methods we will use in our analysis is dimensional reduction. Whenever one of the circles in the problem is very small compared to the other scales, the theory may be approximated by a theory in one dimension less. So, the functional integral of a $(d+1)$-dimensional gauge theory will approximate, in the limit of a very small circumference R_{d+1} for one of the compact circles, that of a d-dimensional gauge theory, with a coupling

[4] Where $W_\mu(\vec{x}) = \frac{1}{N}\langle \mathrm{tr}(Pe^{i \oint A_\mu}) \rangle$ around the circle in the μ direction, for $\mu = 0, 1$.

[5] Actually we should be more careful here — in fact there is no symmetry breaking at finite volume. The closest one can come to a $\mathbb{Z}_N$ symmetry breaking is to have N different saddle points (related by the $\mathbb{Z}_N$ symmetry) dominating the path integral, but the path integral sums over all of them. Thus, there will not really be an expectation value for W_μ, but just for $|W_\mu|^2$ (for example). For the most part we will leave this issue implicit in our discussions.

JHEP01(2006)140

constant $\lambda_d = \lambda_{d+1}/R_{d+1}$. When the small circle has periodic boundary conditions for fermions, the lower-dimensional gauge theory has precisely the same field content as the original theory, except that the zero mode of one of the components of the vector field becomes a scalar field. When the fermions have anti-periodic boundary conditions on the small circle (as for thermal boundary conditions on a temporal circle) they are projected out, leaving only the bosonic fields. Naively, the lower dimensional gauge theory is valid whenever the Kaluza-Klein scale $1/R_{d+1}$ is much larger than the other compactification scales $1/R_i$ and T, and than the dynamical scale $\Lambda_d = \lambda_d^{1/(4-d)}$; the latter condition is the same as $R_{d+1} \ll \lambda_{d+1}^{-1/(3-d)} = 1/\Lambda_{d+1}$.

This argument is naive since an SU(N) gauge theory on a torus actually has excitations whose classical energies scale as $1/(NR_{d+1})$, coming from configurations for which gauge-invariant sets of eigenvalues are periodic only up to a permutation (these configurations play a major role in M(atrix) theory). This scale goes to zero in the 't Hooft large N limit, so naively we can never ignore all the KK modes in this limit. The importance or otherwise of these modes (and so the validity of dimensional reduction) is a dynamical issue determined by the saddle point eigenvalue distribution of the Wilson line operator around the corresponding circle. The light modes described earlier in this paragraph are present only when the Wilson line eigenvalues are spread over the circle (the 'shift' distribution in M(atrix) theory language). When the eigenvalues of the Wilson line operator are sufficiently clumped, these light modes are absent and dimensional reduction is justified. In this paper we will only use dimensional reduction when this criterion is met.

3. Bosonic matrix integrals ($d = 0$)

In this section we briefly review the behavior of bosonic SU(N) matrix integrals; we will find the results of this section useful in our analysis below.

Consider the matrix integral[6]

$$Z = \int \mathcal{D}\Phi_i \exp\left[-\frac{N}{2\lambda_0}\,\mathrm{Tr}\left(\sum_i m_i^2\Phi_i^2 - \sum_{i<j}[\Phi_i,\Phi_j]^2\right)\right]. \tag{3.1}$$

where $i,j = 1,\ldots,p$, ($p > 2$) and the Φ_i are $N \times N$ Hermitean bosonic matrices, in the 't Hooft large N limit in which N is taken to infinity with constant λ_0. Redefining variables $\Phi_i = \frac{\sqrt{\lambda_0}}{m_i}\varphi_i$, we find

$$Z = \int \mathcal{D}\varphi_i \exp\left[-N\,\mathrm{Tr}\left(\sum_i \frac{\varphi_i^2}{2} - \frac{\lambda_0}{2m_i^2m_j^2}\sum_{i<j}[\varphi_i,\varphi_j]^2\right)\right]. \tag{3.2}$$

Let us first study the limit $\lambda_0/m_i^4 \to 0$ (for all i). In this limit the integral factorizes into a product of p identical integrals, each of which is easily solved by saddle points. The saddle

[6]Note that in zero dimensions the only difference between a gauged matrix integral and a non-gauged integral is the volume of SU(N), so we will not need to distinguish the two.

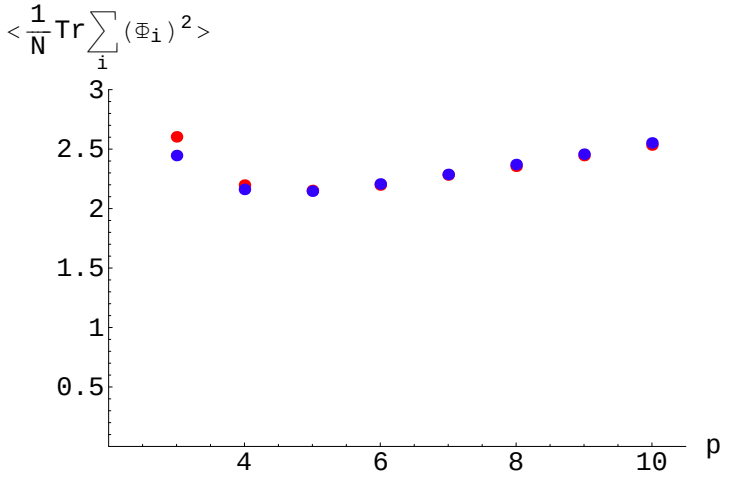

Figure 1: Graph showing $\langle \frac{1}{N} \mathrm{Tr} \sum_i \Phi_i^2 \rangle$ for the massless matrix integral (3.1) with $\lambda_0 = 1$ for various values of p from 3 to 10. The red points correspond to $N = 10$, the blue to $N = 20$.

point eigenvalue distribution for (say) φ_1 is given by the Wigner semi-circle law,

$$\rho(x) = \frac{2}{\pi}\sqrt{1-x^2}, \tag{3.3}$$

and we have

$$\frac{1}{N}\langle \mathrm{tr} \sum_i \Phi_i^2 \rangle = \frac{\lambda_0}{4} \sum_i \frac{1}{m_i^2}. \tag{3.4}$$

In the simple limit considered above, suitably normalized gauge invariant expectation values (like $\frac{1}{N}\mathrm{Tr}\sum_i \Phi_i^2$) are completely determined by a saddle point with sharp edges, and are independent of N. This follows from rather general considerations (factorization and 't Hooft scaling), and so generalizes to most of the systems we study in this paper.

We now turn to the opposite, massless limit of (3.1). It follows from a simple rescaling (similar to the one we used above) that the eigenvalues are localized on a length scale $a = K\lambda_0^{\frac{1}{4}}$ at the corresponding saddle point; Monte Carlo simulations demonstrate that K is of order unity (see appendix A.1 for more details and references), and the values of $\langle \frac{1}{N}\mathrm{Tr}\sum_i \Phi_i^2 \rangle$ are shown in figure 1 for various values of p. Sample eigenvalue distributions which demonstrate a qualitatively similar form to (3.3), including its sharp edge, are shown in figure 2.

It natural to guess that (3.1) is dominated by a saddle point in which the eigenvalues of the scalars are sharply localized for all values of m_i and λ_0. The localization length scale varies smoothly from approximately $\sqrt{\lambda_0}/m$ at large m to approximately $\lambda_0^{\frac{1}{4}}$ at small m. This expectation is easily verified (at sample values of parameters) by a Monte Carlo simulation.

4. Bosonic gauge theories in one dimension

In this section we study the quantum mechanical SU(N) Yang-Mills theory coupled to p

JHEP01(2006)140

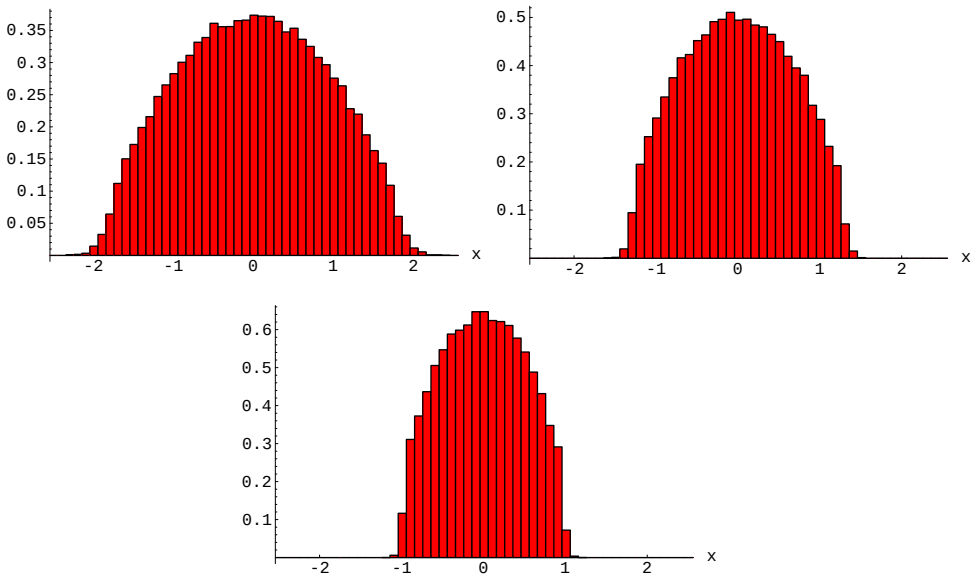

Figure 2: Plots showing the distribution of eigenvalues for the massless matrix integral with $\lambda_0 = 1$ for $p = 3, 5, 10$ (left to right), generated by Monte Carlo simulations for $N = 20$.

adjoint scalar fields ($p \geq 2$), whose Euclidean action is given by

$$S = \frac{N}{2\lambda_1} \int dt \ \mathrm{tr} \left(\sum_i D_0 \Phi_i D_0 \Phi_i + \sum_i M^2 \Phi_i^2 - \sum_{i,j} \frac{1}{2} [\Phi_i, \Phi_j]^2 \right), \tag{4.1}$$

where D_0 is a covariant derivative involving the non-dynamical gauge field A_0, we assumed equal masses for simplicity, and $i, j = 1, \cdots, p$. This theory is believed to possess a unique normalizable vacuum state, and to have a mass gap in its spectrum, at all values of M including $M = 0$. We will study the Euclidean partition function of this theory on a circle of circumference R, which is the same as the thermal partition function of the quantum mechanical system at temperature $T = 1/R$. This theory is characterized by two dimensionless parameters, which we take to be the inverse radius in units of the coupling, $\widetilde{t} = 1/(R\lambda_1^{\frac{1}{3}})$, and the mass in units of the coupling, $m = M/\lambda_1^{\frac{1}{3}}$. In this section we will determine the phase diagram of (4.1) as a function of these parameters.

Two asymptotic regions of this phase diagram are amenable to analytic analysis. First, in the limit of large $\widetilde{t}$, (4.1) effectively reduces to the matrix integral (3.1) (as discussed in section 2); from the analysis of the previous section it then follows that the eigenvalues of the holonomy matrix[7] $U_0 = Pe^{i \oint A_0}$ are clumped at all values of m at large $\widetilde{t}$.

At large m, (4.1) may be analyzed in perturbation theory. In the next subsection we demonstrate that, in this limit, our system undergoes a first order deconfinement transition at $\widetilde{t}_c \sim m/\ln(p)$, and we determine the first correction (in $1/m$) to this phase transition curve. For $\widetilde{t} > \widetilde{t}_c$, the eigenvalues of the Polyakov loop operator are clumped and the $\mathbb{Z}_N$

[7] By an abuse of notation, we will sometimes refer to these as the eigenvalues of the Polyakov loop operator $W_0 = \frac{1}{N} \mathrm{tr}(U_0)$.

invariance is broken. For $\widetilde{t} < \widetilde{t}_c$ the eigenvalues of the Polyakov loop operator are uniformly distributed and $\mathbb{Z}_N$ invariance is restored.

The analysis of the two limits described above (and especially the analytic form of the large m phase transition curve given in the next subsection) suggests that the phase diagram of (4.1) takes the form shown in figures 3 and 4, with the phase boundary extending to some fixed temperature for nonzero mass. In sections 4.2 and 4.3 below, we will use Monte Carlo simulations to plot out this phase diagram in detail, confirming this prediction and giving a quantitative picture of the phase diagram for all values of the mass.

In section 4.4, we discuss the phase diagram for a closely related theory in which one scalar remains massless while the rest have mass M; this theory is relevant to the high temperature limit of 1+1 dimensional gauge theories with massive adjoint scalars (to be discussed in section 5). We find similar qualitative behavior, except that the transition temperature for large mass becomes $\widetilde{t} \sim m/\ln(m)$.

4.1 The large mass limit

When the masses in (4.1) are sufficiently large ($m \gg 1$), (4.1) is weakly coupled at all temperatures, and the thermodynamic behavior can be studied in perturbation theory. As discussed in [1, 2], it is straightforward to integrate out all massive degrees of freedom in the weakly coupled limit to obtain an effective action in terms of the sole light degree of freedom, namely the Wilson line of the gauge field about the circle

$$U = P e^{i \oint_0^R dt A_0} . \tag{4.2}$$

The partition function then takes the form of a unitary matrix model,

$$Z = \int DU e^{-S_{\text{eff}}(U)}, \tag{4.3}$$

where

$$S_{\text{eff}}(U) = p \sum_{n=1}^{\infty} \frac{x^n}{n} \operatorname{tr}(U^n) \operatorname{tr}(U^{\dagger n}) + \mathcal{O}(1/m^3), \tag{4.4}$$

with $x \equiv e^{-MR} = e^{-m/\widetilde{t}}$. In the weak coupling ($m \to \infty$) limit, this matrix model (for $p > 1$) undergoes a large N phase transition as a function of $\widetilde{t}$, from a low $\widetilde{t}$ phase dominated by a saddle point in which the eigenvalues of U are distributed uniformly around the circle, to a high $\widetilde{t}$ phase in which the eigenvalues of U are clumped in the saddle-point configuration.

In the strict $m \to \infty$ limit, the phase transition occurs at the point $\widetilde{t} = m/\ln(p)$, and it is (weakly) of first order. However, as discussed in section 6 of [2], the nature of the phase transition at large but finite m depends on higher order terms in the effective potential, arising from two and three-loop diagrams. In appendix C, we compute the effective action (4.4) to three-loop order, and find that after integrating out all scalars as well as all $n > 1$ Fourier modes of the eigenvalue distribution function (these are all massive near the transition), we are left with an effective action for the lowest Fourier mode

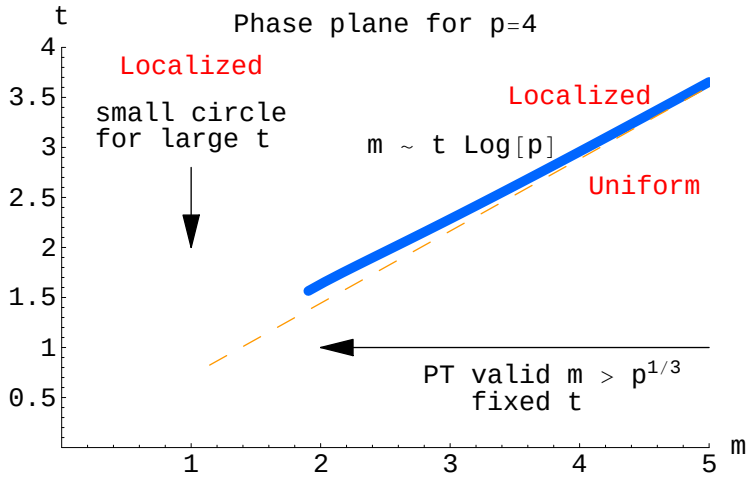

Figure 3: A plot showing the prediction of a first order phase transition at large $m \gg p^{1/3}$ from perturbation theory. The small circle limit suggests localization of the Wilson loop eigenvalues at large $\widetilde{t}$, for fixed m. Then, extrapolating the blue phase boundary would naively indicate that it meets the $\widetilde{t}$ axis.

$u_1 = \frac{1}{N}\,\mathrm{tr}(U)$, of the form

$$S_{\rm eff}(u_1) = N^2(m_1^2(x,1/m^3)|u_1|^2 + \frac{1}{m^6}b(x,1/m^3)|u_1|^4 + \mathcal{O}(1/m^{12})), \tag{4.5}$$

where the leading order expressions for m_1^2 and b are given in appendix C. Since we find $b<0$ at the transition temperature where m_1^2 switches sign, this effective action describes a phase transition which continues to be first order also for large finite m (as at $m\to\infty$) (see [2]), and occurs at the critical temperature

$$\begin{aligned}\widetilde{t}_c = {} & m/\ln(p) + \frac{1}{4m^2}\frac{(p-1)(2p+1)}{p\,\ln(p)} \\ & -\frac{1}{128m^5}\frac{(p-1)}{p^3\,\ln(p)}(\ln(p)(21p^2+6p)+48p^4+20p^3-17p^2-20p-4)+\mathcal{O}(1/m^8),\end{aligned} \tag{4.6}$$

which is slightly below the Hagedorn temperature of this theory.

In summary, when $m \gg p^{\frac{1}{3}}$ (so that perturbation theory is reliable), (4.1) undergoes a first order phase transition at $\widetilde{t}_c$ given by (4.6). For $\widetilde{t} < \widetilde{t}_c$ the Polyakov line eigenvalue distribution is uniform. For $\widetilde{t} > \widetilde{t}_c \approx m/\ln(p)$, the eigenvalues of the Wilson line are clumped.

It is tempting to extrapolate these results beyond the validity of perturbation theory. As displayed in figure 3, plotted for $p=4$, the phase transition line asymptotes to the line $\widetilde{t} = m/\ln(p)$ for large m, and gradually rises above it as m decreases, until perturbation theory is no longer valid (at roughly $m \approx p^{\frac{1}{3}}$). A naive extrapolation of our weak coupling results suggests that the phase transition curve will hit the vertical axis ($m=0$) at a finite temperature.

In the rest of this section we will use Monte Carlo techniques to demonstrate that this guess is indeed correct.

JHEP01(2006)140

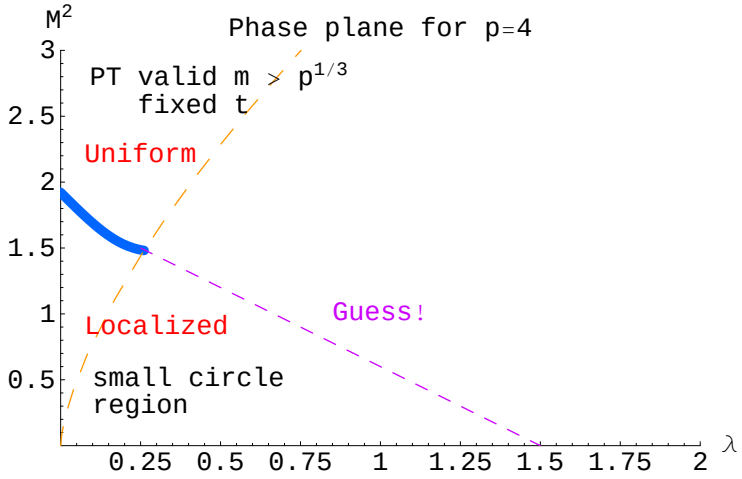

Figure 4: A plot showing the conjectured phase boundary translated into the λ_1, M^2 plane, choosing units with $R = 1$. The Monte Carlo data presented below confirms this picture.

4.2 Results for $m = 0$ from Monte Carlo simulations

The bosonic one-dimensional model (4.1) is rather simple to implement numerically using elementary Monte Carlo methods. In this section we will discuss the numerical results for the behavior of the Wilson line eigenvalues in the cases $p = 2, 4, 9$, characterized by $u_n = \frac{1}{N}|\operatorname{tr}(U^n)|$ (which vanish for all non-zero values of n in the uniform distribution). For these diverse values of p we will see that they all have the same qualitative behavior, and we will link the results to the analytic limits discussed above. Details of the method may be found in appendix E.

In the massless limit, (4.1) is simply the dimensional reduction of the pure SU(N) gauge theory in $(p+1)$ dimensions to one dimension. In this limit (4.1) has a single dimensionless parameter $\lambda_1 R^3 = 1/\widetilde{t}^3$. As we noted above, at large $\widetilde{t}$ this system reduces to the matrix integral of the previous section (with masses set to zero), and so it lies in a phase with a clumped distribution of eigenvalues for the Polyakov line. We now describe results of a Monte Carlo analysis we have performed on this theory.

In figures 5 and 6 we plot the Monte Carlo results for $\langle u_1 \rangle$ and $\langle u_2 \rangle$ in the theory with $p = 9$, for various values of N. These results were previously reported in [3]; as we have reported there, our data strongly suggests a large N transition at $1/\widetilde{t}^3 \simeq 1.4$. As is apparent from figures 5 and 6, the low $\widetilde{t}$ (or large λ_1) phase has $u_1 = 0$ and $u_2 = 0$ (more precisely, u_1 and u_2 are of order $1/N$ for finite N). Clearly, u_1 and u_2 are nonzero (and hence the eigenvalue distribution is non-uniform) in the high temperature phase. All this is perfectly in line with the conjecture made in the previous subsection.

As discussed in [3], we have not been able to clearly resolve the order of the phase transition studied in this subsection. Unfortunately, the phase transition of our system appears to lie very near the boundary between first and second order behavior (see [3]). In this situation it is difficult to numerically distinguish between the two reasonable possibilities (see appendix E), which are either a first order phase transition or a second order

JHEP01(2006)140

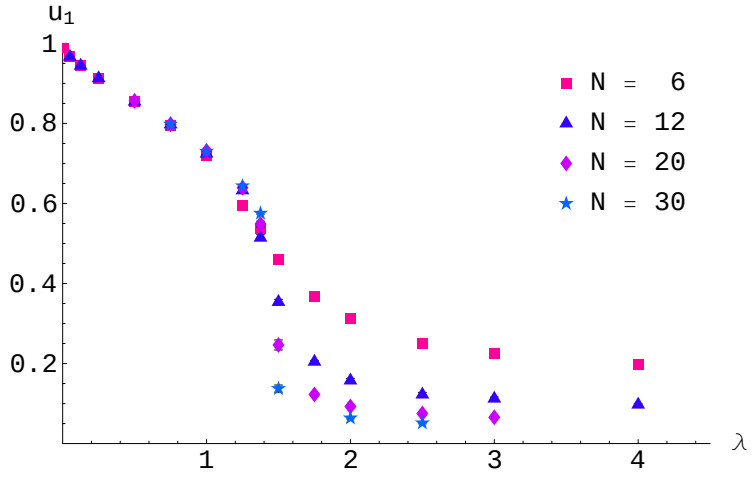

Figure 5: Figure of $\langle u_1 \rangle$ as a function of λ_1 for $p = 9$ with various values of N. We choose units with $R = 1$, and thus $\lambda_1 = 1/\widetilde{t}^3$. We see that as N increases the points to the right of $\lambda_1 \simeq 1.4$ appear to decrease, consistent with $1/N$ scaling. To the left of this value the points appear to tend to a limiting curve. This indicates a sharp discontinuity in u_1 at infinite N, with u_1 being an order parameter. Statistical error bars are comparable to the point sizes.

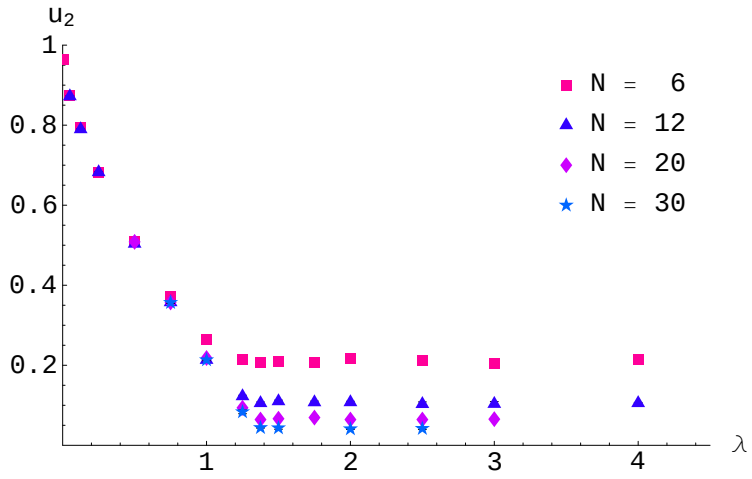

Figure 6: Figure of $\langle u_2 \rangle$ as a function of λ_1 for $p = 9$ with various values of N. Again a discontinuous behavior is indicated in the large N limit. As above, we choose $R = 1$ units.

phase transition followed by another, third order phase transition [2]. However, it is clear from the data that if the second scenario is correct then the two phase transitions must be very close together.

We have repeated the analysis of this section at $p = 2, 4$. We find qualitatively identical behavior to that reported in the previous paragraphs, but this time with the phase transition at $\lambda_{crit} R^3 = 1/\widetilde{t}_c^3 \simeq 0.4, 0.9$, respectively.

JHEP01(2006)140

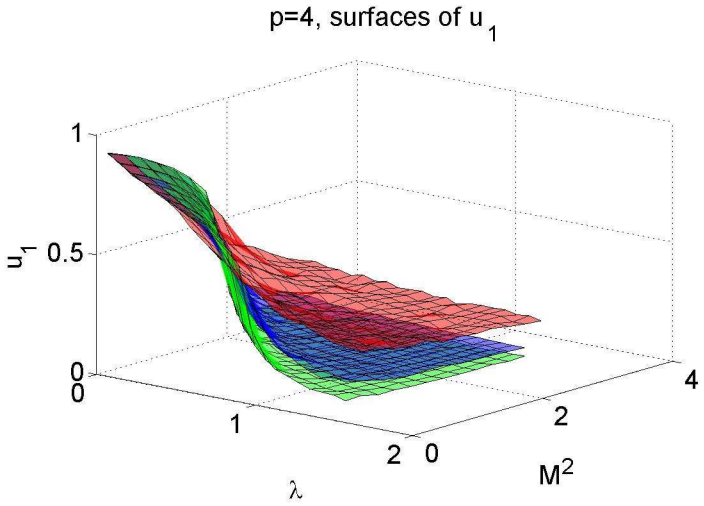

Figure 7: Figure of $\langle u_1 \rangle$ in the λ_1, M plane (in $R = 1$ units). The red (top) surface is for $N = 6$, blue is $N = 12$ and green (bottom) $N = 20$. We see a transition line bounding the origin where outside the line u_1 decreases with increasing N (approximately consistent with $1/N$ scaling), and inside the line a limit is approached. The transition line appears to connect the massless transition to the large m transition. The black mesh of the surfaces gives the sampling density. Thus, the (small) statistical error can be seen as the 'roughness' of the surface.

4.3 Monte Carlo simulations with non-zero mass

We have also performed Monte Carlo simulations of (4.1), as a function of $\widetilde{t}$, at various different values of m. The results of these simulations (which we present in this subsection) smoothly interpolate between the analytic prediction of subsection 4.1 and the $m = 0$ results of the previous subsection, allowing us to fill out the phase diagram of (4.1) and to confirm the guess displayed in figure 4.

In figures 7 and 8 we present three dimensional plots of $\langle u_1 \rangle$ and $\langle u_2 \rangle$ as functions of $\lambda_1 R^3 = 1/\widetilde{t}^3$ and $MR = m/\widetilde{t}$, for the case $p = 4$ [8]. An examination of figures 7 and 8 reveals that the $m, \widetilde{t}$ plane may be divided into two regions. In the first (uniform) region u_1 and u_2 decrease as N increases; this decrease is approximately fit by a $1/N$ decay to zero. In the second (clumped) region u_1 and u_2 asymptote to fixed, m and $\widetilde{t}$ dependent, nonzero values. These two regions are divided by a transition line. As in the case of $m = 0$, u_1 appears to jump discontinuously (or at least with a very sharp slope) across this transition line in the limit $N \to \infty$.

In figures 9, 10, 11 we plot this transition line as a function of m and $\widetilde{t}$ (see below for more details on how exactly this transition line was obtained from our data). In each case this line interpolates smoothly between the analytic prediction of subsection 4.1 and the results of the previous subsection. As in the previous subsection, our numerics are unable

[8] These graphs are best viewed in colour.

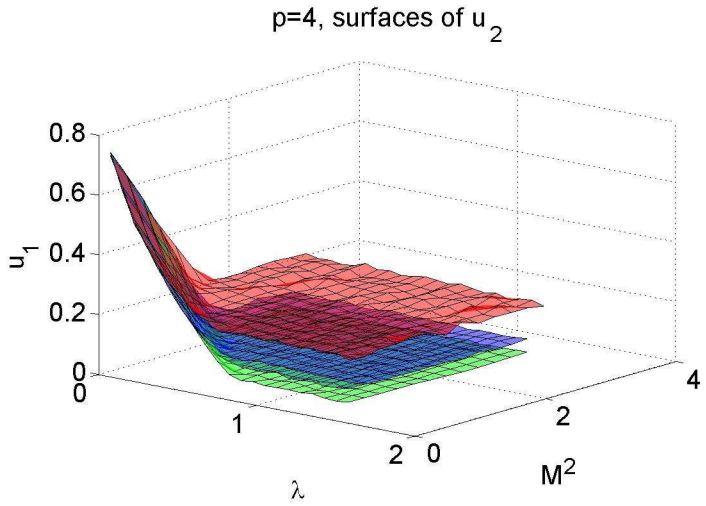

Figure 8: Figure of $\langle u_2 \rangle$ in the λ_1, M plane, employing the same conventions as in the previous figure.

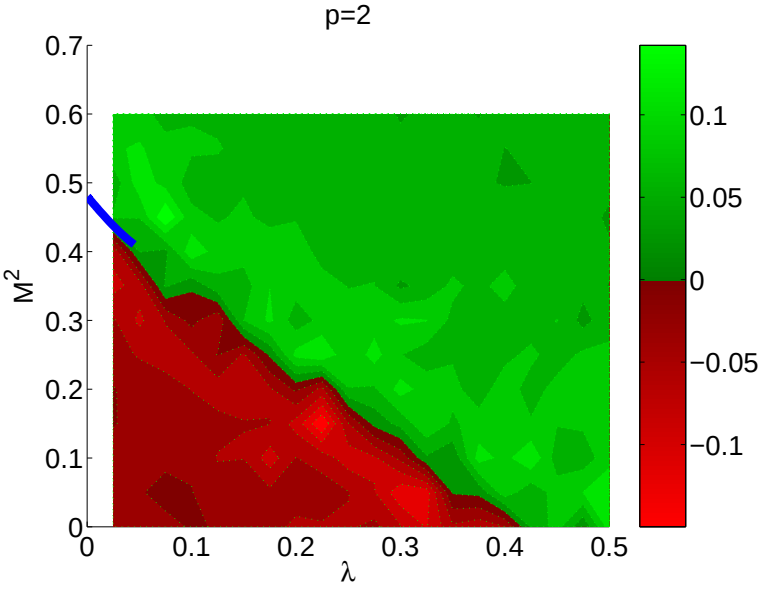

Figure 9: Contours of $\Delta^{12,20}\langle u_1 \rangle$ for the $p = 2$ theory, in the λ_1, M plane (in $R = 1$ units). The green region is predicted to be in the uniform eigenvalue phase, and the red region in the localized phase. The blue curve gives the large m perturbative prediction, where the perturbative expansion is valid. We clearly see that the phase boundary connects the two axes.

to definitively establish the order of the transition; however they are certainly consistent with the simplest conjecture, which is that the transition (which the computations of

JHEP01(2006)140

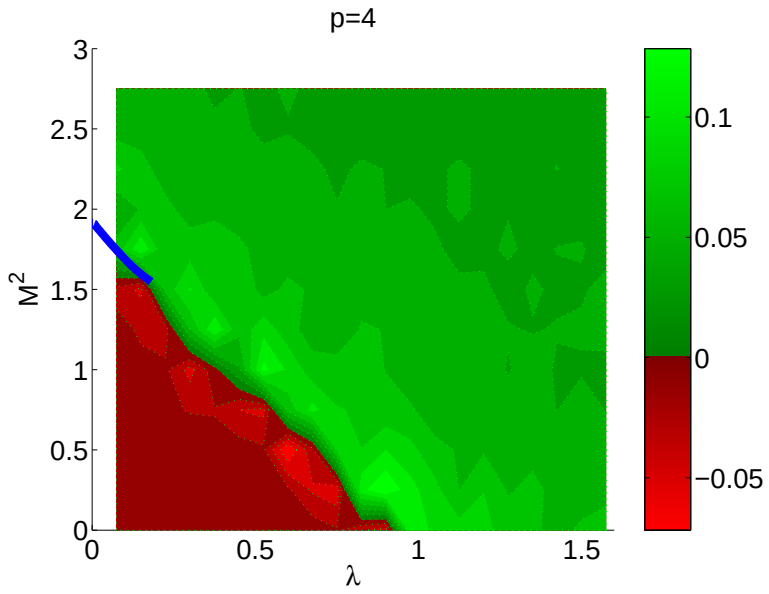

Figure 10: Contours of $\Delta^{12,20}\langle u_1\rangle$ for the $p = 4$ theory, with the same conventions as above.

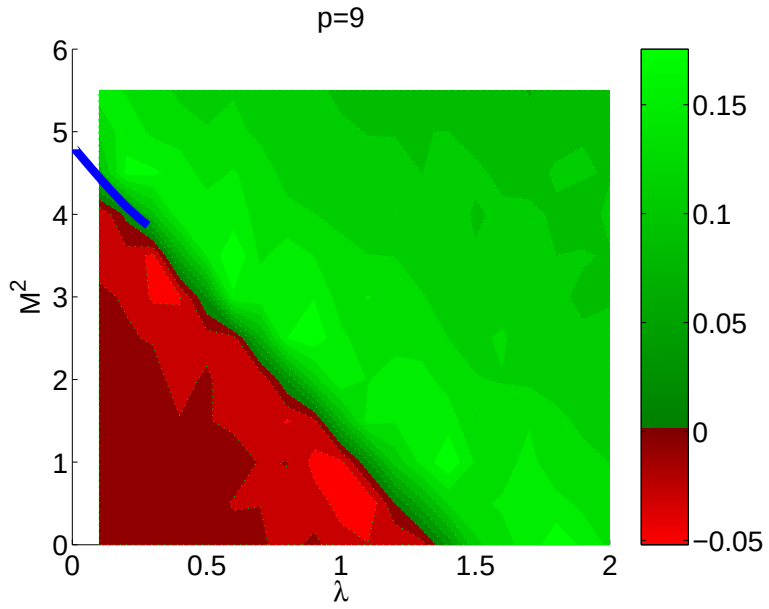

Figure 11: Contours of $\Delta^{6,12}\langle u_1\rangle$ for the $p = 9$ theory, with the same conventions as above.

subsection 4.1 have established to be of first order at large m) remains of first order for all values of m.

To end this subsection we give a precise definition of the transition lines plotted in figures 9, 10, 11. We characterize the position of the transition by computing the difference

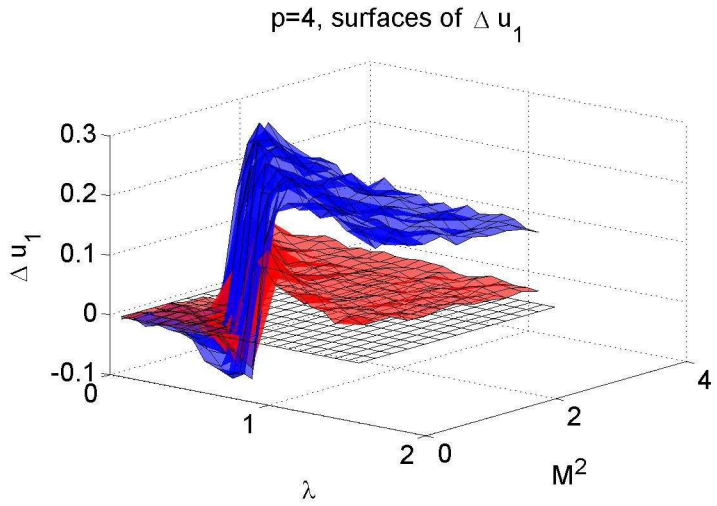

Figure 12: Figure of $\Delta^{6,20}\langle u_1\rangle$ (blue) and $\Delta^{12,20}\langle u_1\rangle$ (red) in the λ_1, M plane for the $p = 4$ theory (taking $R = 1$ units). We take the zero contour to measure the position of the phase boundary.

between the values of $\langle u_1\rangle$ for different values of N. 'Outside' the phase transition boundary u_1 decreases with increasing N, while 'inside' it stays roughly constant (with a small increase). We may estimate the phase boundary as the line where these differences are zero, namely the function u_1 is neither increasing nor decreasing with increase of N. Of course, this estimate to the phase transition line becomes more accurate as we increase N.

To illustrate our procedure, in figure 12 we plot $\Delta^{6,20}\langle u_1\rangle \equiv \langle u_1\rangle^{(N=6)} - \langle u_1\rangle^{(N=20)}$ and $\Delta^{12,20}\langle u_1\rangle \equiv \langle u_1\rangle^{(N=12)} - \langle u_1\rangle^{(N=20)}$. Both surfaces in the plot give a consistent phase boundary location.

4.4 One massless and p massive scalars

Before concluding this section, we briefly consider a generalization of (4.1) for which one of the scalars (which we call ϕ) remains at zero mass, while the other p scalars are massive. This arises in studying the high temperature limit of a 1+1 dimensional gauge theory with massive scalars, for which the temporal component of the gauge field leads to a massless scalar in the dimensionally reduced theory.

The theory behaves in a qualitatively similar manner to the massive theory considered above. For $m \to 0$, the two theories are the same, while at large m, we will see that both theories have a phase boundary at a temperature which goes to infinity as m goes to infinity, though with different dependence on m.

In this limit, it is again appropriate to integrate out the massive scalars at one loop to generate an effective potential for ϕ and the holonomy matrix U. The ϕ independent terms will be given by (4.4) as before, with corrections negligible as long as $m \gg p^{1/3}$. At

very large m, the most important ϕ-dependent term will be a mass term[9]

$$S_{\text{eff}} = \int dt \frac{\lambda_1 p}{2M} \operatorname{tr}(\phi^2). \tag{4.7}$$

The leading ϕ^4 interaction comes with a coefficient $g_\phi^2 \sim \lambda_1^2/NM^3$, and can be ignored relative to the quadratic terms when integrating out ϕ as long as

$$m_\phi/(g_\phi^2 N)^{\frac{1}{3}} \gg 1 \qquad \Rightarrow \qquad m \gg 1. \tag{4.8}$$

There will be additional terms involving both ϕ and U, but these are nonlocal and will be suppressed exponentially by powers of e^{-RM} for large R. We should be able to ignore these if

$$RM \gg 1 \qquad \Rightarrow \qquad \widetilde{t} \ll m. \tag{4.9}$$

When all these conditions are satisfied, we may integrate out the scalar ϕ at one loop (using only the kinetic term and mass term) to obtain additional terms in the effective action for U. The result (including terms we have already from integrating out the scalars of mass M) is

$$S_{\text{eff}}(U) = \sum_{n=1}^{\infty} \frac{1}{n}(px^n + x^{n\epsilon}) \ \operatorname{tr}(U^n) \operatorname{tr}(U^{\dagger n}), \tag{4.10}$$

where $x = e^{-MR} = e^{-m/\widetilde{t}}$ as before and ϵ is the ratio of the induced ϕ mass to the X masses,

$$\epsilon = \frac{\sqrt{p}}{m^{\frac{3}{2}}} \ll 1. \tag{4.11}$$

This theory has a deconfinement phase transition when

$$\begin{aligned} & px + x^\epsilon = 1 \\ \Rightarrow \quad & px + \epsilon \ln(x) = 0 \\ \Rightarrow \quad & x = \frac{\epsilon}{p}\left(\ln\left(\frac{p}{\epsilon}\right) + \mathcal{O}\left(\ln\left(\ln\left(\frac{p}{\epsilon}\right)\right)\right)\right) \\ \Rightarrow \quad & \widetilde{t} = \frac{2}{3}\frac{m}{\ln(m)}\left(1 + \mathcal{O}\left(\frac{\ln(\ln(m))}{\ln(m)}\right)\right). \end{aligned} \tag{4.12}$$

Note that at this temperature, (4.8) and (4.9) are both satisfied, so our analysis is self consistent. Thus, we conclude that at large m, the phase transition temperature goes as $\widetilde{t} = \frac{2}{3}m/\ln(m)$.

5. Two dimensional bosonic gauge theories on T^2

In this section we study the two dimensional large N SU(N) Yang-Mills theory coupled to p Hermitian scalar fields in the adjoint representation,

$$S = \frac{N}{2\lambda}\int d^2x \ \operatorname{tr}\left\{F_{12}^2 + \sum_I \left[\left(\partial_\mu \Phi^I - i\left[A_\mu, \Phi^I\right]\right)^2 + m_I^2 \Phi_I^2\right] - \sum_{I<J}\left[\Phi^I, \Phi^J\right]^2\right\}, \tag{5.1}$$

[9]Here, ϕ is normalized to have a kinetic term $\int dt \operatorname{tr}(\frac{1}{2}(D_0\phi)^2)$.

with $I, J = 1, \cdots, p$. Viewed as a $1+1$ dimensional quantum field theory, this theory is believed to possess a unique normalizable vacuum state and a Hagedorn growth in its density of states (see [8] for the special case $p = 1$). We will study the partition function of the Euclidean theory on a rectangular torus with radii R_1 and R_2, as a function of the geometry and masses (in units where the coupling is fixed). We will investigate this system in two separate limits; first when all scalars are massless, and second when all scalars have large mass.

In this case, the geometry has two non-contractible cycles, so any saddle point configuration will be characterized by two holonomy matrices which we call U and V. At each point in parameter space, we will ask whether the eigenvalues of these matrices in the saddle point configuration are clumped or unclumped (uniformly distributed on the unit circle), and so obtain a phase diagram containing four possible phases. The phase diagram will turn out to be similar in the massless and large mass limits, and so we believe it is likely to have the same structure for any value of the mass.

5.1 The massless theory

We first consider the theory (5.1) in the limit where the scalar masses are zero. We wish to understand the phase diagram of this theory on a rectangular torus, as a function of its two dimensionless parameters, which we can choose to be $r_1 = R_1\sqrt{\lambda}$ and $r_2 = R_2\sqrt{\lambda}$, the circumferences of the spatial and temporal circles in units where the coupling is set to one. Since there is nothing to distinguish the two circles, the phase diagram must be symmetric under the exchange $r_1 \leftrightarrow r_2$.

Let us first review what we know about the theory in the limit $r_1 \to \infty$ keeping r_2 fixed; this limit gives the decompactified system at a temperature $1/R_2$. At low temperatures this system is believed to confine, with a Hagedorn tower of glueball states (see [8] for a proof for the case $p = 1$). As the temperature is raised, the system undergoes a sharp deconfinement transition at a temperature of order $\sqrt{\lambda}$. In Euclidean space the order parameter for this phase transition is the expectation value of the Wilson line around the x_2 circle; the eigenvalues of this Wilson line are clumped at high temperatures but uniformly smeared over the circle at low temperatures. Thus, for large r_1, we expect a deconfinement transition line which asymptotes to a constant r_2 of order unity. Exchanging the two circles, we must then have also a phase transition line for large r_2 asymptoting to constant r_1, across which the eigenvalues of the Wilson line in the x_1 direction clump as we decrease r_1.

We now turn to the opposite limit where the spatial circle R_1 is very small. When the Kaluza-Klein scale $1/R_1$ is much larger than the scale $\lambda_1^{1/3}$ set by the effective one-dimensional coupling $\lambda_1 = \lambda/R_1$ and also much larger than the temperature $1/R_2$, the theory will reduce to the one-dimensional theory considered in the previous section with $p+1$ massless scalars. The parameter $\widetilde{t}$ of the previous section is given in terms of the two-dimensional parameters by

$$\widetilde{t} = \frac{1}{R_2 \lambda_1^{\frac{1}{3}}} = \frac{r_1^{\frac{1}{3}}}{r_2}. \tag{5.2}$$

Thus, in the regime $r_1 \ll 1$ and $r_1 \ll r_2$ we expect a phase transition along the curve

$$r_2 = \frac{1}{\widetilde{t}_c^{(p+1)}} r_1^{\frac{1}{3}} \tag{5.3}$$

where $\widetilde{t}_c^{(p+1)}$ is the critical value of $\widetilde{t}$ in the one-dimensional theory with $p+1$ massless scalars. The eigenvalues of U (the holonomy around R_2) will be clumped or unclumped for values of r_2 below or above this line (again assuming that $r_1 \ll 1$ and $r_1 \ll r_2$).

Again, we may swap the role of the two circles and conclude that there is an additional phase transition along the curve

$$r_2 = (\widetilde{t}_c^{(p+1)})^3 r_1^3 \tag{5.4}$$

such that the eigenvalues of V (the holonomy around R_1) are clumped/unclumped above/ below the curve, in the regime of validity $r_2 \ll r_1$ and $r_2 \ll 1$.

Note that these results rely on the numerics of the previous section, however, in the regime

$$r_1^{\frac{1}{3}} \gg r_2 \gg r_1^3 \tag{5.5}$$

all non-zero modes are weakly coupled and can be integrated out at one loop (see appendix A) so we are able to verify analytically that both U and V are clumped in this regime.[10]

Putting all this together, we conclude that the phase diagram of (5.1) for $m \gg 1$ takes the form shown in figure 13. We have sketched three possible simple completions of this phase diagram, however, our current lack of understanding of the dynamics at $r_1, r_2 \sim 1$ prevents us from distinguishing between these three possibilities.

The phase transitions in figure 13 are driven by the strongly coupled dynamics of a field theories' worth of degrees of freedom, and so are difficult to analytically control. In the following subsections, we will see that as for the one-dimensional theories considered in section 4, analytic analysis becomes possible in the opposite limit when the scalar masses become large, $m \gg 1$, where we take $m_I = M$ and define the dimensionless mass parameter $m = M/\sqrt{\lambda}$.

5.2 $M = \infty$

First, consider the strict limit $M \to \infty$. In this limit all scalar fields may simply be set to zero and (5.1) reduces to pure two dimensional Yang-Mills theory on a torus, an exactly solvable system. Over 30 years ago [9], Migdal rewrote the partition function of two dimensional Yang-Mills theory on a torus in terms of an integral over the two unitary holonomy matrices

$$Z_{ym} = \int DU\, DV \sum_R d_R e^{-\frac{\tilde{\lambda}}{2N} C_2(R)} \chi_R(UVU^{-1}V^{-1}), \tag{5.6}$$

[10] Naively, we might expect that the theory should admit a perturbative analysis as long as the torus area is small in units of the coupling. In fact, as in finite temperature computations in 3+1 dimensional theories, this naive expectation is modified by infrared effects (see [3] for a discussion of this point). The correct regime of validity may be obtained by requiring that the R_1 circle should be small in units of the one-dimensional coupling λ/R_2 and that the R_2 circle should be small in units of the one-dimensional coupling λ/R_1, leading to (5.5).

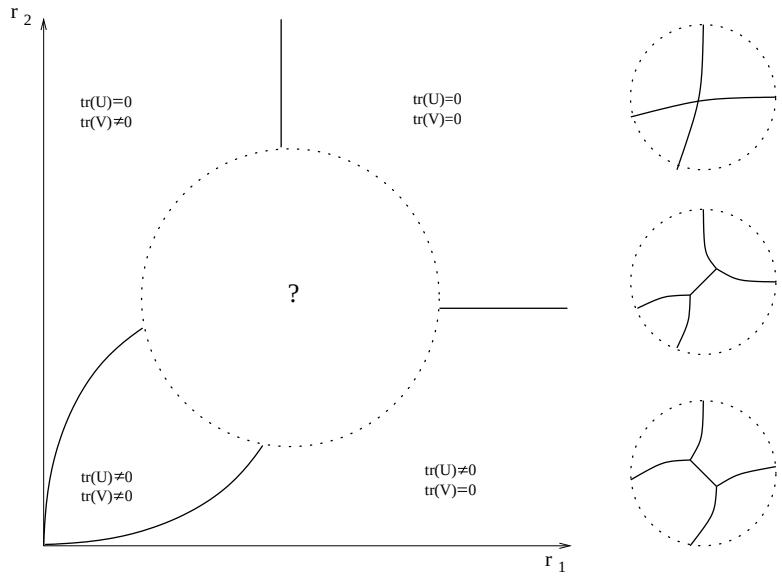

Figure 13: Known aspects of the phase diagram of massless bosonic SU(N) gauge theories with three possible completions. U is the expectation value of the holonomy in the x_2 direction, and V is the expectation value of the holonomy in the x_1 direction.

where

$$\widetilde{\lambda} = \lambda R_1 R_2 = r_1 r_2. \tag{5.7}$$

Here, the sum over R runs over all representations of the SU(N) gauge group, and d_R and $C_2(R)$ are the dimension and the quadratic Casimir of the representation R (see appendix D for a brief derivation). It is not difficult to integrate out one of the two matrices — say, V — in (5.6), to obtain an effective action for U,

$$Z_{ym} = \int DU \sum_R e^{-\frac{\widetilde{\lambda}}{2N} C_2(R)} \chi_R(U) \chi_R(U^\dagger) \ , \tag{5.8}$$

which may be evaluated to obtain [10 – 13]

$$Z_{ym} = \sum_R e^{-\frac{\widetilde{\lambda}}{2N} C_2(R)} \ . \tag{5.9}$$

For our analysis below, it will be useful to note (see appendix D) that at large N, (5.8) may be written as

$$Z_{YM} = \int DU \ \exp\left(\sum_n \frac{1}{n} (-e^{-\widetilde{\lambda} n} + 2 e^{-\frac{\widetilde{\lambda} n}{2}}) \, \mathrm{tr}(U^n) \, \mathrm{tr}(U^{-n}) \right) . \tag{5.10}$$

Equation (5.10) may be rewritten as an integral over the moments of the eigenvalue density function as

$$Z_{YM} = \int du_n d\bar{u}_n \ \exp\left(-N^2 \sum_n \frac{1}{n} (e^{-\frac{\widetilde{\lambda} n}{2}} - 1)^2 |u_n|^2 \right) , \tag{5.11}$$

where the moments, u_n, are related to U by

$$u_n \equiv \frac{1}{N} \operatorname{tr}(U^n). \tag{5.12}$$

Note that the coefficients of $|u_n|^2$ in (5.11) are positive for all n; it follows that Z_{YM} is dominated by the saddle point $u_n = 0$ for all n, in which the eigenvalue distribution is uniform. Of course, the same result is true for the eigenvalues of the holonomy matrix V. Thus we conclude that, independent of the torus radii, the eigenvalues of both holonomy matrices are unclumped for pure Yang-Mills theory on T^2.

Notice that at small $\widetilde{\lambda}$ the effective mass for u_n in (5.11) is very small (the mass squared is approximately $n\widetilde{\lambda}^2/4$). As a consequence, in this regime a small attractive perturbation could cause the eigenvalues to clump. We will now argue that such a perturbation is supplied by the effective potential generated by scalar fields Φ_I at large but finite mass.

5.3 Large M, noncompact limit

We first note that when R_1 is larger than any other length scale in the problem, the theory should behave like the noncompact thermal 1+1 dimensional theory with very massive scalars. This theory was analyzed in [14]. There, it was argued that by integrating out all degrees of freedom except the spatially dependent holonomy matrix (in the R_2 direction) $U(x)$, the system reduces to the model

$$S = \int dx \left\{ \frac{N}{2\lambda R_2} \operatorname{tr}(|\partial_x U|^2) - p\sqrt{\frac{M}{2\pi R_2}} e^{-MR_2} \operatorname{tr}(U(x)) \operatorname{tr}(U^\dagger(x)) \right\} . \tag{5.13}$$

Using collective field theory methods, they showed that this model displays a first order deconfinement transition at a temperature corresponding to

$$r_2 = \frac{2}{m} \ln(m) \left(1 + \mathcal{O}\left(\frac{\ln(\ln(m))}{\ln(m)} \right) \right) . \tag{5.14}$$

Thus, our model will have a phase transition curve asymptoting to this value for large r_1. Above the curve (corresponding to the noncompact theory at low temperatures), the eigenvalues of the temporal holonomy U will be unclumped, while below it, they will be clumped. By symmetry, there must be an additional phase boundary asymptoting to $r_1 \sim \frac{2}{m} \ln(m)$ at large r_2, across which the eigenvalues of the spatial holonomy V clump.

5.4 Large M, small volume

We may now ask about the opposite limit, where R_1 is so small that the theory is effectively one-dimensional. Assuming that the eigenvalues of V are clumped (we will see that this is the case for small enough R_1), the theory will behave as a one dimensional theory with p massive scalars and one massless scalar (from the spatial component of the gauge field) as long as the Kaluza-Klein scale $1/R_1$ is much larger than the mass M, the temperature $1/R_2$ and the scale $\sqrt{\lambda}$ of the gauge theory, yielding conditions

$$r_1 \ll r_2, \qquad r_1 \ll 1/m, \qquad r_1 \ll 1. \tag{5.15}$$

Here, the last relation is implied by the second for large m.

In the language of section 4, the corresponding one-dimensional theory will have parameters $\widetilde{t} = r_1^{\frac{1}{3}}/r_2$ and $m_1 = m r_1^{\frac{1}{3}}$. From the results of section 4.4, we expect that this theory undergoes a phase transition at some $\widetilde{t}_c(m_1)$ for all values of m_1, where $\widetilde{t}_c$ rises from some value $\widetilde{t}_c^{(p+1)}$ of order one for small m_1 and asymptotes to $2m_1/(3\ln(m_1))$ for large m_1. Expressing these results in terms of our two-dimensional parameters, we predict a phase transition at

$$r_2 = \frac{r_1^{\frac{1}{3}}}{\widetilde{t}_{c(m r_1^{\frac{1}{3}})}} \tag{5.16}$$

which gives

$$r_1 = \begin{cases} r_2^3 (\widetilde{t}_c^{(p+1)})^3 & r_1 \ll \frac{1}{m^3} \\ \frac{r_2^2}{pm} e^{2m r_2} & \frac{1}{m^3} \ll r_1 \ll \frac{1}{m} \end{cases} \tag{5.17}$$

where to derive the last expression we used the equation in the second line of (4.12). For larger values of r_1, the conditions (5.15) are no longer satisfied, so the theory is no longer well approximated by a one-dimensional theory.

The transition line (5.17) separates a region with clumped U eigenvalues (for smaller r_2) from a region with unclumped U eigenvalues (for larger r_2). By symmetry, we will have an addition phase boundary separating regions of clumped and unclumped V eigenvalues, obtained by the replacement $r_1 \leftrightarrow r_2$ in (5.17).

5.5 Large M, intermediate radius

At intermediate values of R_1, neither of the approximations so far apply, but the theory is still simple enough to treat analytically as long as the scalar masses are very large. In this case, we can reliably integrate out the scalars at one-loop order, leading to an effective action

$$S = \frac{N}{2\lambda} \left(\int d^2x \ \mathrm{tr}(F_{12}^2) \right) + \frac{p}{2} \ln \det(-D_\mu^2 + M^2) \tag{5.18}$$

for the gauge fields. The explicit expression for the determinant will in general be quite complicated, with local terms built from the gauge field strength and its covariant derivatives, together with non-local terms involving the Wilson lines about the spatial and temporal cycles. The former will be small relative to the tree-level F^2 term as long as $m \gg 1$. The non-local terms involving the holonomy around a cycle fall off exponentially with the radius of the cycle in units of the inverse scalar mass, but we will see that these terms are important even when this exponential is very small (equal to an inverse power of m).

For sufficiently small R_1 and R_2 (we will be more explicit below), terms involving the spatially varying modes of the fields will be suppressed, and it is enough to consider the effective action assuming that the components A_1 and A_2 of the gauge field (and hence the holonomy matrices) are spatially constant. In appendix B, we show that up to commutator terms, the result for the effective action in this case is

$$S_{\text{eff}} = \frac{p}{2} \ln \det(-D_\mu^2 + M^2)$$

$$= -p \sum_{(k,n)\neq(0,0)} \mathrm{tr}(U^n V^k)\,\mathrm{tr}(U^{-n}V^{-k}) M R_1 R_2 \frac{K_1\left(M\sqrt{R_1^2k^2+R_2^2n^2}\right)}{2\pi\sqrt{R_1^2k^2+R_2^2n^2}} \tag{5.19}$$

$$\to -p \sum_{(k,n)\neq(0,0)} \mathrm{tr}(U^n V^k)\,\mathrm{tr}(U^{-n}V^{-k}) \sqrt{M} R_1 R_2 \frac{\exp\left(-M\sqrt{R_1^2k^2+R_2^2n^2}\right)}{2\sqrt{2\pi}(R_1^2k^2+R_2^2n^2)^{\frac{3}{4}}},$$

where in the last line we have taken the limit of large MR_i and used the asymptotic form of the associated Bessel function K_1.[11] Note that if MR_1 and MR_2 are both sufficiently large, all terms will be small relative to the $(k,n)=(0,\pm1)$ and $(k,n)=(\pm1,0)$ terms. In addition, the commutator terms that we have not written necessarily involve at least two powers of U and two powers of V, so we expect them to be suppressed at least as strongly as the U^2V^2 terms above.

Thus, when the spatially varying modes can be ignored and both MR_1 and MR_2 are large, the effective action from the scalars is well approximated by

$$S_{\text{eff}}(U,V) = f(U) + g(V), \tag{5.20}$$

where

$$\begin{aligned} f(U) &= -\frac{p}{\sqrt{2\pi}}\frac{R_1}{R_2}\sqrt{MR_2}e^{-MR_2}\,\mathrm{tr}(U)\,\mathrm{tr}(U^\dagger)\,, \\ g(V) &= -\frac{p}{\sqrt{2\pi}}\frac{R_2}{R_1}\sqrt{MR_1}e^{-MR_1}\,\mathrm{tr}(V)\,\mathrm{tr}(V^\dagger)\,. \end{aligned} \tag{5.21}$$

Note that f comes from the second term in (5.13) if we take the integral to run over a finite range R_1 and ignore the non-zero modes of $U(x)$. Both the kinetic term and the potential term in (5.13) will produce quadratic terms in the non-zero modes of $U(x)$. By demanding that the relative coefficient for the potential term is small, we obtain an explicit condition for when the non-zero modes of $U(x)$ may be ignored,[12]

$$r_1^2 \ll \frac{1}{\sqrt{mr_2}} e^{mr_2}. \tag{5.22}$$

Similarly, the non-zero modes of $V(x)$ can be ignored when

$$r_2^2 \ll \frac{1}{\sqrt{mr_1}} e^{mr_1}. \tag{5.23}$$

When all of our assumptions apply, the partition function becomes (using (5.18) and (5.6))

$$Z_{ym} = \int DU\,DV \sum_R d_R e^{-\frac{\tilde{\lambda}}{2N}C_2(R)} \chi_R(UVU^{-1}V^{-1}) e^{-f(U)} e^{-g(V)}. \tag{5.24}$$

[11] When U and V commute, this is precisely a pairwise potential between the N points on the dual torus formed by the simultaneous eigenvalues of U and V.

[12] This condition is most appropriate in the regime $r_1 \gg r_2$ where (5.13) is valid, but this is the only place we will need it in what follows. Similarly, the equation for the non-zero modes of $V(x)$ is the appropriate condition for the regime $r_2 \gg r_1$.

Making the change of variables $U \to WUW^{-1}$ for unitary W, and integrating over W (more details in appendix D), we find

$$Z_{ym} = \int DU\, DV \sum_R e^{-\frac{\tilde{\lambda}}{2N} C_2(R)} \frac{d_R^2}{d_R^2 - 1} e^{-f(U)} e^{-g(V)} \tag{5.25}$$
$$\left\{ -1 + \chi_R(V)\chi_R(V^\dagger) + \chi_R(U)\chi_R(U^\dagger) - \frac{1}{d_R^2}\chi_R(U)\chi_R(U^\dagger)\chi_R(V)\chi_R(V^\dagger) \right\}.$$

For large N, the coefficient $d_R^2/(d_R^2 - 1)$ can be set to one.

From this expression, we would like to understand the behavior of our order parameters, $\ln(Z_{ym})/N^2$ and the expectation values for the temporal and spatial Wilson loops. We note first that for the purposes of computing the partition function or any observable depending on either U or V alone, the last term in (5.25) can be ignored relative to the other terms as long as $R_1 M$ and $R_2 M$ are large enough. For, suppose we evaluate the partition function with an operator $\mathcal{O}(U)$ inserted. Then in the last two terms of (5.25), the V dependent terms may be collected inside the U integral to obtain

$$\int DV\; e^{-g(V)} \left\{ 1 - \frac{1}{d_R^2}\chi_R(V)\chi_R(V^\dagger) \right\} = Z_g \left\{ 1 - \langle \frac{1}{d_R^2}\chi_R(V)\chi_R(V^\dagger) \rangle_g \right\}. \tag{5.26}$$

Here, Z_g and $\langle\rangle_g$ are the partition function and expectation values for the unitary matrix model with action $g(V)$. But as long as the coefficient in $g(V)$ is small,

$$r_2 \ll \frac{1}{p}\sqrt{\frac{r_1}{m}} e^{m r_1}\ , \tag{5.27}$$

such a model will be dominated by the repulsive eigenvalue potential from the measure, and display confining behavior with a uniform eigenvalue distribution for the saddle point. In this case, the expectation value in (5.26) will vanish for large N, since this is just the norm squared of the Polyakov loop in the representation R. In other words, term by term in the sum over R in (5.25), the contribution from the last term will be negligible relative to the contribution from the third term. Similarly, if we insert any operator $\mathcal{O}(V)$, the last term will be negligible compared to the second term as long as

$$r_1 \ll \frac{1}{p}\sqrt{\frac{r_2}{m}} e^{m r_2}\ . \tag{5.28}$$

Let us now assume that both (5.27) and (5.28) are satisfied and consider first the partition function (5.25) with no operator inserted. We then obtain

$$Z_{YM} = -Z_{M=\infty} Z_g Z_f + Z_f Z_{S_\infty(V)+g} + Z_g Z_{S_\infty(U)+f} \tag{5.29}$$

where $Z_{M=\infty}$ is the partition function (5.9) for the pure Yang-Mills theory, and S_∞ is the action in the expression (5.8) for the pure Yang-Mills partition function reduced to a single matrix integral. Now, $Z_{M=\infty}$, Z_g, Z_f are all finite for large N (when our conditions are satisfied) since they correspond to confining theories, so Z_{YM} will show deconfined behavior if and only if either $Z_{S_\infty(V)+g}$ or $Z_{S_\infty(U)+f}$ does.

Using the large N result (5.10) to get an explicit expression for S_∞ and rewriting in terms of the modes of the eigenvalue distribution, we find

$$Z_{S_{\infty(U)+f}} = \int du_n d\bar{u}_n \exp\left(-N^2 \sum_n \frac{1}{n}(1 - e^{-\frac{r_1 r_2 n}{2}})^2 |u_n|^2 + N^2 \frac{p}{\sqrt{2\pi}} \frac{r_1}{r_2} \sqrt{m r_2} e^{-m r_2} |u_1|^2 \right). \tag{5.30}$$

We see that the scalar effective potential gives a negative contribution to the mass squared for the lowest Fourier mode of the eigenvalue distribution. Thus, u_1 becomes tachyonic, and the free energy in (5.30) becomes of order N^2, when

$$\frac{p}{\sqrt{2\pi}} \frac{r_1}{r_2} \sqrt{m r_2} e^{-m r_2} > (1 - e^{-\frac{r_1 r_2}{2}})^2. \tag{5.31}$$

Since we assumed that the left-hand side is very small, this can only happen when $r_1 r_2 \ll 1$. Similarly, $Z_{S_\infty(V)+g}$ will show deconfining behavior when

$$\frac{p}{\sqrt{2\pi}} \frac{r_2}{r_1} \sqrt{m r_1} e^{-m r_1} > (1 - e^{-\frac{r_1 r_2}{2}})^2. \tag{5.32}$$

These two curves intersect at

$$r_1 = r_2 = \frac{4}{m} \ln(m) \left(1 + \mathcal{O}\left(\frac{\ln(\ln(m))}{\ln(m)} \right) \right), \tag{5.33}$$

and together form part of the boundary of the region with free energy of order one and both U and V unclumped. Note that the curve (5.31) exits the region where (5.22) is satisfied when $r_1 \sim m/\ln(m^2)$ and r_2 has decreased to be of order $2\ln(m)/m$. Beyond this, we cannot trust the functional form (5.31) of the curve, but we have already argued in section 5.4 that there should be a phase boundary asymptoting to precisely this value, suggesting that our result (5.31) matches on smoothly to the large R_1 behavior (and similarly for (5.32)). Noting that $r_1 r_2 \ll 1$ on the curve (5.31) everywhere that (5.22) is satisfied, we can write a more explicit expression for the phase boundary in this region,

$$\begin{aligned} r_1 &= \frac{4p}{\sqrt{2\pi}} \frac{\sqrt{m}}{r_2^{\frac{5}{2}}} e^{-m r_2} \qquad r_1 < r_2 \ll \frac{1}{r_1} \\ r_2 &= \frac{4p}{\sqrt{2\pi}} \frac{\sqrt{m}}{r_1^{\frac{5}{2}}} e^{-m r_1} \qquad r_2 < r_1 \ll \frac{1}{r_2} \end{aligned} \tag{5.34}$$

Note that the conditions (5.27) and (5.28) are satisfied for all such values.

To see what happens on the deconfined side of this boundary, let us now understand the behavior of the order parameters $\langle |\operatorname{tr}(U)|^2/N^2 \rangle$ and $\langle |\operatorname{tr}(V)|^2/N^2 \rangle$, focusing for now on the first one. As we have argued above, the last term in (5.25) can be ignored in computing either of these, so by the arguments leading to (5.29), we obtain

$$\langle \frac{1}{N^2} |\operatorname{tr}(U)|^2 \rangle = \frac{-Z_{M=\infty} Z_g Z_f \langle |u_1|^2 \rangle_f + Z_f Z_{S_\infty(V)+g} \langle |u_1|^2 \rangle_f + Z_g Z_{S_\infty(U)+f} \langle |u_1|^2 \rangle_{S_\infty(U)+f}}{-Z_{M=\infty} Z_g Z_f + Z_f Z_{S_\infty(V)+g} + Z_g Z_{S_\infty(U)+f}} \tag{5.35}$$

Now, in the region of interest, at least one of $Z_{S_\infty(U)+f}$ or $Z_{S_\infty(V)+g}$ behaves as $\exp(cN^2)$ so the first terms in both the numerator and denominator (which are at most of order one in N) will be completely negligible here. In the remaining expression,

$$\langle \frac{1}{N^2} |\operatorname{tr}(U)|^2 \rangle = \frac{Z_f Z_{S_\infty(V)+g} \langle |u_1|^2 \rangle_f + Z_g Z_{S_\infty(U)+f} \langle |u_1|^2 \rangle_{S_\infty(U)+f}}{Z_f Z_{S_\infty(V)+g} + Z_g Z_{S_\infty(U)+f}} \tag{5.36}$$

even when both $Z_{S_\infty(U)+f}$ and $Z_{S_\infty(V)+g}$ have $\exp(cN^2)$ behavior, the larger will completely dominate in both numerator and denominator, so

$$\langle \frac{1}{N^2} |\operatorname{tr}(U)|^2 \rangle = \begin{cases} \langle |u_1|^2 \rangle_f = 0 & Z_{S_\infty(V)+g} > Z_{S_\infty(U)+f} \\ \langle |u_1|^2 \rangle_{S_\infty(U)+f} \neq 0 & Z_{S_\infty(U)+f} > Z_{S_\infty(V)+g} \end{cases} \tag{5.37}$$

The model with larger magnitude for the free energy will be the one for which the $|u_1|$ mode is more tachyonic, and by inspection of (5.21), this will be the $S_\infty(U) + f$ model for $R_1 > R_2$ and the $S_\infty(V) + g$ model for $R_2 > R_1$.

Thus, from (5.37) and the analogous result for $\langle |v_1|^2 \rangle = \langle |\operatorname{tr}(V)|^2/N^2 \rangle$, we conclude that there is a phase boundary at $r_1 = r_2$ starting from curve (5.34) and continuing towards the origin, such that the eigenvalues of U are clumped and the eigenvalues of V are unclumped for $R_1 > R_2$ while the opposite is true for $R_2 > R_1$. This phase boundary cannot continue all the way to the origin, since we have argued in section 5.5 that both sets of eigenvalues are clumped for small enough $r_1 = r_2$. Indeed, in ignoring the higher order terms in (5.19), we have assumed that $R_1 M$ and $R_2 M$ are large, so we can only say with certainty that the phase boundary exists in the region $1/m \ll r_1 = r_2 < 4\ln(m)/m$. For smaller values of r, the phase boundary must bifurcate symmetrically, and we expect that the two curves thus produced connect smoothly onto the two phase boundaries which we argued in section 5.4 emanate from the origin.

5.6 Summary of the large mass theory

Combining all of our results, we conclude that the phase diagram for large N Yang-Mills theory with very massive adjoint scalars compactified on a rectangular torus appears as in figure 14. Here, solid lines indicate regions where we have been able to determine the analytic form of the phase boundary. Note that this diagram displays the same qualitative behavior as one of the possible completions of the massless phase diagram (figure 13), so it seems reasonable to speculate that the phase structure is qualitatively identical for all values of the scalar masses.

In figure 15, we present an alternate version of the diagram, with axes labeled by the size of the spatial circle in units of the coupling ($r_1 = R\sqrt{\lambda}$) and the temperature in units of the spatial radius ($TR = r_1/r_2$). Analogous units were used in our analysis [2, 15] of 3+1 dimensional Yang-Mills theory on a sphere, where our analysis suggested a single first order transition extending from large volume to a finite value of TR in the zero volume limit. In the present case, it is interesting to note that:

1. The solid line corresponding to deconfinement as measured by the temporal Wilson loop expectation value is not smooth.

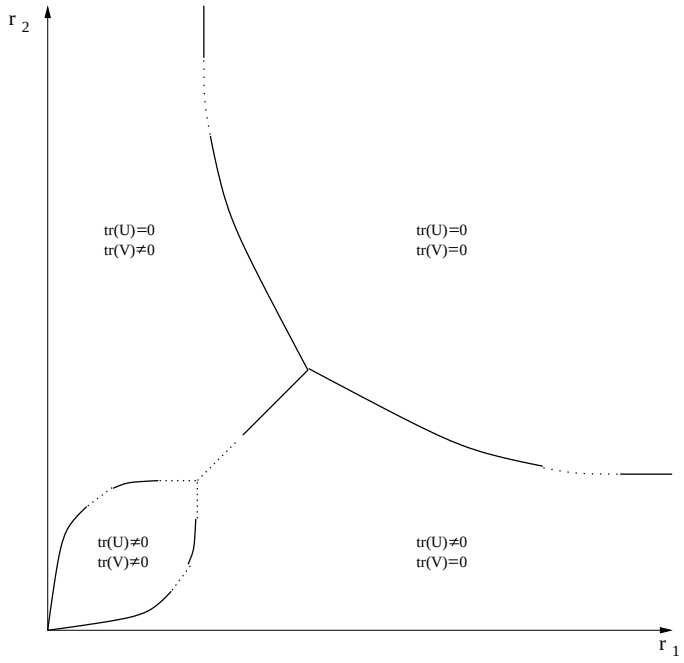

Figure 14: Phase diagram for Euclidean two-dimensional Yang-Mills theory with massive adjoint scalars on T^2. Solid lines indicate phase boundaries for which we have analytic expressions.

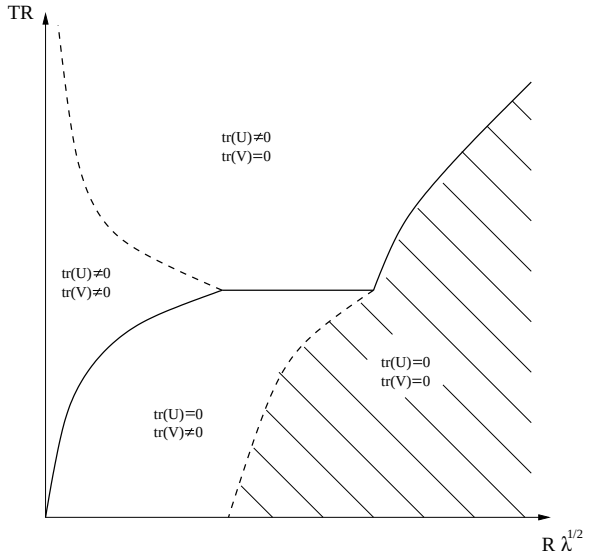

Figure 15: Phase diagram for 1+1 dimensional Yang-Mills theory with massive adjoint scalars on S^1. The free energy is of order one in the shaded region and of order N^2 elsewhere.

2. While the deconfinement transition does extend all the way to zero volume as for the topologically trivial case, the transition temperature does not approach a finite value in units of the inverse spatial radius.

3. The large volume regions for both the confined and deconfined regions are separated

by phase transitions from the small volume regions.

4. The two order parameters for confinement, $1/N^2$ times the free energy and the expectation value of the Polyakov loop, do not have the same behavior at small and large volumes in this example. More specifically, in the "confined" region below the solid line, the free energy is of order one at large volume, but it becomes of order N^2 to the left of the dotted line.

6. Maximally supersymmetric quantum mechanics

In the rest of this paper we will study one and two dimensional maximally supersymmetric gauge theories on circles and tori. As is well known, Yang-Mills theories with 16 supercharges display rather different dynamics from their bosonic counterparts; in particular the scalar effective potential in these theories has flat directions, and the spectrum of these theories is not gapped. As a consequence we expect (see section 2) that the phase diagrams of these theories (which we will obtain) will differ in significant aspects from the equivalent diagrams for the purely bosonic theories of the previous sections.

Partition functions of supersymmetric theories on tori are strongly dependent on the boundary conditions of the fermions around cycles of the tori. When all fermions are periodic, the path integral is localized on supersymmetric configurations (and computes a Witten Index [16]). These path integrals depend weakly (if at all) on parameters, and do not undergo phase transitions. In this paper we will focus on the dynamically more interesting path integrals with anti-periodic boundary conditions for fermions; these are relevant in particular for studying finite temperature.

In this section we consider the maximally supersymmetric SU(N) Yang-Mills theory in one dimension, in the 't Hooft large N limit[13]. The Euclidean Lagrangian is given by

$$S = \frac{N}{\lambda_1}\int dt\ \mathrm{tr}\left(\frac{1}{2}D_0\Phi_i D_0\Phi_i + \frac{i}{2}\Psi^\dagger D_0\Psi - \frac{1}{4}[\Phi_i,\Phi_j]^2 + \frac{1}{2}\Psi^\dagger\gamma^i[\Phi_i,\Psi]\right), \tag{6.1}$$

where $i,j = 1,\cdots,9$ and Ψ is a real 16 component spinor. The time direction is identified with a period $\beta = 1/T$; the bosonic fields are periodic in this direction and the fermions are anti-periodic. The theory may be characterized by the single dimensionless parameter $\widetilde{t} = T/\lambda_1^{1/3}$, in terms of which the effective dimensionless 't Hooft coupling is $1/\widetilde{t}^3$.

As the fermions are anti-periodic about the circle, all fermion modes acquire large masses as the circle shrinks to zero size, so in the small radius or large $\widetilde{t}$ limit, our theory behaves identically to the bosonic theory considered in section 3; in particular, the eigenvalues of the holonomy matrix are clumped on the circle.

In the opposite, small $\widetilde{t}$, limit the quantum mechanics is strongly coupled; but in this case, we can use a dual description to understand the dynamics.

[13]It is important to distinguish this from the M(atrix) theory large N limit [17], which is conjectured to describe the light-cone quantization of a flat-space gravitational theory (M-theory) and has a different thermodynamic behavior.

We recall that the 't Hooft limit of massless maximally supersymmetric 0+1 dimensional Yang-Mills theory is believed [18, 19] to be dual to type IIA string theory in the near horizon limit of the extremal black D0-brane solution of type IIA string theory. This background has a reliable description in terms of type IIA supergravity (small curvatures in string units and weak string coupling) for a range of the radial coordinate corresponding to energy scales $E \ll \lambda_1^{1/3} = (g_1^2 N)^{\frac{1}{3}}$ in the quantum mechanics.[14]

Similarly, the finite temperature quantum mechanics in the 't Hooft limit should be dual to a near-extremal version of this geometry. This dual geometry contains a horizon, and type IIA supergravity is a valid description near the horizon as long as $\widetilde{t} \ll 1$. The presence of a horizon in the Lorentzian geometry implies a contractible thermal circle in the associated Euclidean geometry. Thus, the expectation value of the (traced) Wilson line around the circle in the gauge theory, which is mapped in the string theory (after adding to it some dependence on scalar fields) to the action of a string worldsheet ending on the thermal circle [20 – 22] is non-zero. This implies that the eigenvalue distribution is non-uniform.

Therefore, for the massless supersymmetric theory, the eigenvalues of the Wilson line operator seem to be clumped (or at least non-uniformly distributed) at both large and small values of $\widetilde{t}$, so the phase transition that we found in the bosonic theory appears to be absent here.

This disparity of behavior between the bosonic and supersymmetric theories at low temperatures should not come as a surprise; indeed, their zero temperature dynamics is completely different. In the purely bosonic theory, the classical flat directions in the potential are completely removed by quantum fluctuations which result in a linear potential between the spatial eigenvalues. The resulting spectrum should be discrete. On the other hand, for the supersymmetric theory, the quantum fluctuations generate only the well-known $\dot{x}^4/|x|^7$ potential between eigenvalues, and the spectrum is continuous.

As for the bosonic theory, we can consider more generally a massive deformation. The simplest such deformation has equal masses for all scalars and fermions (of course, this breaks supersymmetry). In the limit of large mass, all fermion and scalar modes are weakly coupled, so as for the bosonic theory, we may integrate out the matter at one loop to reduce the partition function to a unitary matrix model. The result is similar to (4.6), but with $p = 17$ (assuming that all fields have the same mass). Thus, for large enough masses, we again have a phase transition from clumped eigenvalues at large $\widetilde{t}$ to a uniform distribution for small $\widetilde{t}$, with $\widetilde{t}_c = m/\ln(17) + \mathcal{O}(1/m^2)$. Since we have a phase transition for $\widetilde{t} \approx m/\ln(17)$ at large m and no phase transition at $m = 0$, it must be that the phase transition line intersects the $\widetilde{t} = 0$ axis either at $m = 0$ or at some small non-zero value of m. There is certainly a qualitative change in the theory as soon as a mass is turned on, since the zero temperature potential goes from being flat asymptotically (with a corresponding continuous spectrum) to asymptotically harmonic (with a discrete spectrum). While this motivates a possible phase transition, it is not clear how to directly relate this information to the behavior of our order parameter.

[14] For large but finite N, the type IIA supergravity description is also no longer valid at low energies, when $E \ll g_1^{2/3} N^{1/7}$, but this scale goes to zero in the 't Hooft large N limit.

7. Maximally supersymmetric Yang-Mills theory on T^2

In this section, we would like to study the thermodynamics of maximally supersymmetric 1+1 dimensional Yang-Mills theory on a circle, corresponding to the Euclidean theory on T^2. In this case, the fermions are anti-periodic about the thermal circle, but we have a choice between anti-periodic and periodic boundary conditions for the spatial circle. In fact, we will see that both possibilities are included if we make the natural generalization to non-rectangular tori.

7.1 General tori: classification and fundamental regions

In this subsection we will classify and describe the inequivalent tori on which maximally supersymmetric Yang-Mills theory can be compactified. We specify our torus by two identifications:

$$z \sim z + L \sim z + L\tau \tag{7.1}$$

(where $\tau = \tau_1 + i\tau_2$ is the modular parameter), and further specify that all fermions are anti-periodic around both of these cycles. Below we will denote the holonomy along the cycle $z \sim z + L$ as V and the holonomy along $z \sim z + L\tau$ as U. The phase diagram we wish to determine is a function of three real dimensionless variables: the complex variable τ and the dimensionless coupling constant $\widetilde{\lambda} = g_{YM}^2 NA$, where $A = L^2\tau_2$ is the area of the torus.

Bosonic Yang-Mills theories on tori whose τ parameters are related by an $\mathrm{SL}(2,\mathbb{Z})$ transformation ($\tau \to (a\tau + b)/(c\tau + d)$ with integers a, b, c, d satisfying $ad - bc = 1$) are identical at equal values of $\widetilde{\lambda}$. It is thus sufficient to study such theories in the familiar $\mathrm{SL}(2,\mathbb{Z})$ fundamental domain, denoted by the region I in figure 16.

The supersymmetric Yang-Mills theory we will study in this section includes fermions; the partition function for this theory will be identical (at equal values of $\widetilde{\lambda}$) only on those tori that are related by the subgroup of $\mathrm{SL}(2,\mathbb{Z})$ that preserves our fermion boundary conditions. This group is generated by $\tau \to -1/\tau$ and $\tau \to \tau + 2$. The fundamental domain for this subgroup is the union of the regions I, II and IV in figure 16. In this section we will study the Yang-Mills partition function on tori with modular parameters lying in this fundamental domain.

To end this subsection we comment on the physical interpretation of tori in regions II and IV. Tori on the two vertical lines that border the diagram in figure 16 have modular parameters of the form $\tau = \pm 1 + i\tau_2$ (with real τ_2). These tori are best thought of as rectangular tori with $\tau' = i\tau_2$, with periodic boundary conditions on fermions along the τ' cycle (the fermion boundary conditions remain anti-periodic along the '1' cycle). In general, a torus in the region IIb/a with modular parameter τ may be thought of as a torus in the region I, with $\tau' = \tau \pm 1$ and periodic boundary conditions along the τ' cycle. Similarly, a torus in the region IVb/a may be reinterpreted as a torus in the region I with $\tau' = -1/(\tau \pm 1)$ and periodic boundary conditions along the '1' cycle.

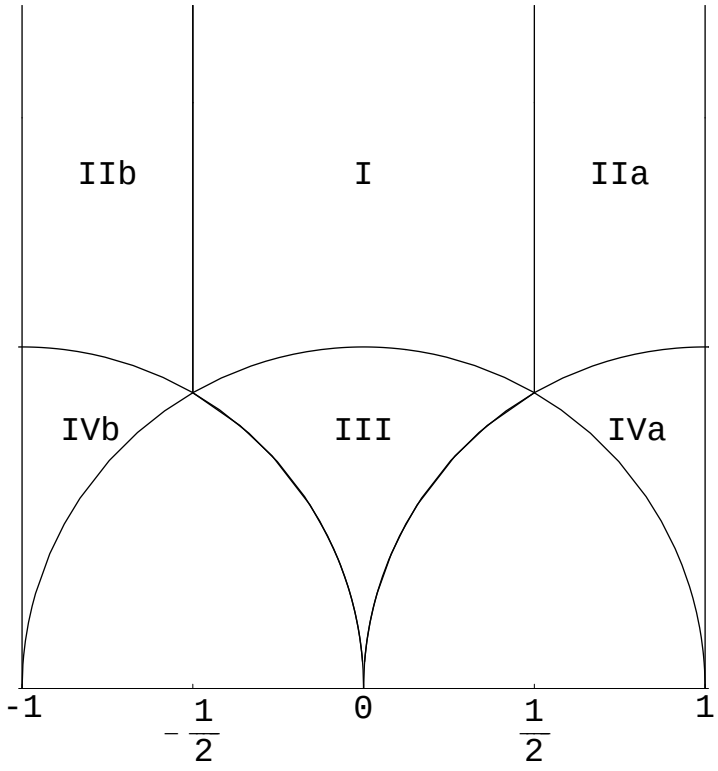

Figure 16: Fundamental region of the modular group for a theory with fermions.

7.2 Analysis at small $\widetilde{\lambda}$

As discussed in previous sections, at small $\widetilde{\lambda}$ the Kaluza Klein modes of the field theory on T^2 may reliably be integrated out at one loop, provided that $\widetilde{\lambda}/M^4$ is small, where M is the mass of the lightest KK mode in units in which the area of the torus is one. When this integrating out is legitimate, the resulting determinant (see appendix A) ensures that the eigenvalues for both holonomies U and V clump.

Expanding all fields (take a scalar field $\phi(z)$ as an example) on the torus in Fourier modes subject to the periodicity $\phi(z) = \phi(z + L) = \phi(z + L\tau)$ gives

$$\phi(z) = \sum_{m,n=-\infty}^{\infty} \phi_{m,n} \exp\left[\frac{2\pi i}{L\tau_2}\left(\tau_2 m \mathrm{Re}(z) + (n - \tau_1 m)\mathrm{Im}(z)\right)\right], \tag{7.2}$$

leading to $M^2 = \frac{4\pi^2}{\tau_2}\left(m^2|\tau|^2 + n^2 - 2mn\tau_1\right)$ (in units of $1/L$). For bosonic fields m and n are integers, while for fermions $m + 1/2$ and $n + 1/2$ are integers.

In regions I and II the lightest non-zero-mode for scalars is the $(m = 0, n = \pm 1)$ mode with $M^2 = 4\pi^2/\tau_2$. So, we can integrate out all the KK modes at one loop reliably in regions I and II if

$$\widetilde{\lambda}\tau_2^2 \ll 1. \tag{7.3}$$

For larger values of τ_2 all modes with $m \neq 0$ (the boundary conditions ensure that this includes all the fermions) are still very heavy and decouple, so we can study the theory

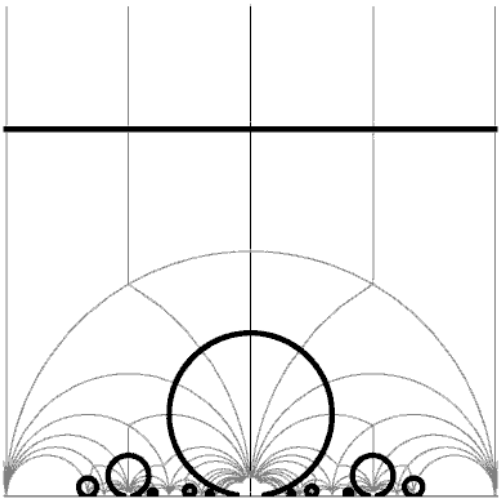

Figure 17: The phase transition line at $\tau_2 \sim 1/\sqrt{\widetilde{\lambda}}$ and its images, for a specific value of $\widetilde{\lambda}$.

by including only the $m = 0$ modes. The resulting quantum mechanical theory is simply the bosonic quantum mechanics of section 4, with $R = L\tau_2$ and coupling $\lambda_1 = \lambda/L$, giving an effective dimensionless coupling $\widetilde{\lambda}\tau_2^2$. It follows from the analysis of section 4 that the system undergoes a phase transition at $\tau_2 = a/\sqrt{\widetilde{\lambda}}$, where a is a number of order unity, determined in the analysis of section 4. At larger values of τ_2 one of the $\mathbb{Z}_N$ symmetries of the system is restored, and $\langle \mathrm{tr}(U) \rangle = 0$.

In region IVa the lightest mode is $(m = n = \pm 1)$, with mass

$$M^2 = \frac{4\pi^2}{\tau_2}\left((1-\tau_1)^2 + \tau_2^2\right) \tag{7.4}$$

(the IVb region is related to this by $(\tau_1 \to -\tau_1, m \to -m)$). The KK modes are weakly coupled and can be integrated out provided that

$$\frac{\widetilde{\lambda}\tau_2^2}{((1-\tau_1)^2+\tau_2^2)^2} \ll 1. \tag{7.5}$$

When (7.5) is not obeyed (but still $\widetilde{\lambda} \ll 1$), all modes with $n \neq m$ become very heavy and decouple. The resulting effective quantum mechanical theory of the light modes includes fermions, and is, in fact, precisely the one dimensional supersymmetric quantum mechanics of section 6. We have argued that it is unlikely that this system undergoes a phase transition. It seems that our system is in the $\langle \mathrm{tr}(U) \rangle \neq 0, \langle \mathrm{tr}(V) \rangle \neq 0$ phase throughout region IV.

Mapping regions I and II by the (allowed) modular transformations we find an infinite number of images of the phase transition line $\tau_2 = a/\sqrt{\widetilde{\lambda}}$, which are drawn in figure 17. For example, in region III this line is mapped by the $\tau \to -1/\tau$ transformation to the line $(\tau_2' - \sqrt{\widetilde{\lambda}}/2a)^2 + \tau_1'^2 = \widetilde{\lambda}/4a^2$. Above this line both holonomies are clumped, $\langle \mathrm{tr}(U) \rangle \neq 0$ and $\langle \mathrm{tr}(V) \rangle \neq 0$, while below the line (in region III) $\langle \mathrm{tr}(V) \rangle = 0$.

To summarize, a torus is characterized by its modular parameter τ. If we scale the 't Hooft coupling constant appropriately then the partition function of the theory is a modular invariant function on the τ plane. Thus, we only need to study it in the fundamental region (which is different from the standard one because of the fermions). In this region we find a single phase transition line where the eigenvalues of the Wilson loop along the longer fundamental cycle clump. This line has an infinite number of images on the τ plane through modular transformations. Above we gave the results for the case of two anti-periodic cycles for the fermions, but the case of one periodic cycle (corresponding, in particular, to the finite temperature theory) is simply related to this by $\tau \to \tau + 1$.

7.3 Strong coupling from AdS/CFT

When the effective coupling $\widetilde{\lambda}$ is large, the theory cannot be analyzed using perturbative techniques, but we can use the AdS/CFT correspondence to study the phase structure of the system.

The dual of the $1+1$ dimensional maximally supersymmetric Yang-Mills theory in the 't Hooft large N limit is the near-horizon geometry of the D1-brane metric of type IIB string theory [19]. If we put the gauge theory on a spatial circle of circumference L then the dual theory is obtained by a periodic identification of the spatial coordinate. If we want to study the theory at temperature T we have to consider the near extremal D1-brane solution. The relevant Euclidean string frame metric and dilaton are:

$$ds^2 = \alpha' \left[\frac{u^3}{\sqrt{d_1 \lambda'}} \left(1 - \frac{u_0^6}{u^6}\right) \frac{dt'^2}{L^2} + \frac{u^3}{\sqrt{d_1\lambda'}} \frac{d\theta'^2}{(2\pi)^2} + \frac{\sqrt{d_1\lambda'}}{u^3 \left(1 - \frac{u_0^6}{u^6}\right)} du^2 + u^{-1}\sqrt{d_1\lambda'} d\Omega_7^2 \right], \tag{7.6}$$

$$e^{\phi} = 2\pi \frac{\lambda'}{N} \sqrt{\frac{d_1\lambda'}{u^6}}, \tag{7.7}$$

where $\lambda' = \lambda L^2, d_1 = 2^6\pi^3, u_0^2 = \frac{16\pi^{5/2}}{3} TL\sqrt{\lambda'}$, we have to identify $t' \sim t' + 1/T$ to avoid the conical singularity at $u = u_0$, and the periodicity of θ' is 2π. There is also a 3-form field which we do not explicitly write down. Defining $\rho = TL$ and changing coordinates to $t = t'T$ and $\theta = \frac{\rho\theta'}{2\pi}$, we can write the metric in the form:

$$ds^2 = \alpha' \left[\frac{u^3}{\sqrt{d_1\lambda'}\rho^2} \left[\left(1 - \frac{u_0^6}{u^6}\right) dt^2 + d\theta^2 \right] + \frac{\sqrt{d_1\lambda'}}{u^3 \left(1 - \frac{u_0^6}{u^6}\right)} du^2 + u^{-1}\sqrt{d_1\lambda'} d\Omega_7^2 \right], \tag{7.8}$$

with $u_0^2 = \frac{16\pi^{5/2}}{3}\rho\sqrt{\lambda'}$. Now, defining a complex coordinate $z = t + i\theta$, we have the identifications $z \sim z + 1 \sim z + i\rho$, and the conformal boundary of this geometry is a rectangular T^2. The parameter ρ appears both in the identifications and explicitly in (7.8), but in fact we can get rid of it in the metric by noting that the form of (7.8) is invariant under a rescaling $u \to \alpha u, u_0 \to \alpha u, \lambda' \to \alpha^2\lambda', \rho \to \alpha\rho$. If we use this rescaling with $\alpha = \rho^{-1}$ we can rewrite (7.8) as

$$ds^2 = \alpha' \left[\frac{u^3}{\sqrt{d_1\widehat{\lambda}}} \left[\left(1 - \frac{u_0^6}{u^6}\right) dt^2 + d\theta^2 \right] + \frac{\sqrt{d_1\widehat{\lambda}}}{u^3 \left(1 - \frac{u_0^6}{u^6}\right)} du^2 + u^{-1}\sqrt{d_1\widehat{\lambda}} d\Omega_7^2 \right], \tag{7.9}$$

with $\widehat{\lambda} = \lambda'/\rho^2$ and $u_0^2 = \frac{16\pi^{5/2}}{3}\sqrt{\widehat{\lambda}}$. Since now ρ appears only in the identifications, it is clear that if we change the identifications to $z \sim z+1 \sim z+\tau$ with $\tau = \tau_1 + i\tau_2$ an arbitrary complex number, we still have a solution to IIB supergravity (with the same u_0) without any singularities, whose asymptotic boundary is a torus of modular parameter τ.

If we want to compute the thermal partition function of the field theory living on the boundary we have to consider all supergravity (or more generally string theory) solutions X_i with the appropriate behavior at infinity. The partition function of the dual gauge theory in the large N limit is:

$$Z_{\text{gauge}} = \sum_i \exp(-I(X_i)), \tag{7.10}$$

where I is the Euclidean action of the supergravity (string theory) solution.

Let's say that we want to compute the partition function of supersymmetric Yang-Mills (SYM) theory on a torus of modular parameter τ_f. It is clear that solutions of the form (7.9) contribute to the partition function only if the asymptotic T^2 of the supergravity solution can be conformally mapped to the T^2 on which the gauge theory lives. This is possible if and only if the modular parameter of the torus of the gravity τ_g is related to τ_f by some modular transformation. So we have to start from the supergravity solution with $\tau_g = \tau_f$, consider all modular transformations of τ_g, and then sum the exponentials of the Euclidean action of the corresponding supergravity solutions [23, 24].

In general all solutions will contribute to the partition function. But we notice that the Euclidean action scales as N^2, so in the large N limit we get the dominant contribution from the solution with the smallest Euclidean action. This allows for sharp phase transitions in the $N \to \infty$ limit, if the solution with the minimum action changes discontinuously as we vary the parameters of the theory.

If we try to compute the Euclidean action of any of the solutions we find that it diverges as we integrate over all space. However we are not interested in the value of the action but in comparing the action of different solutions. One way to compare the actions is to match the solutions (metric and other fields) at some large cutoff value of the radius, calculate the action difference and then send the value of the cutoff to infinity. The divergent terms cancel once the geometries are properly matched, and one obtains a finite result. Alternatively one can add counter-terms to cancel the divergences, leading to equivalent results.

Before we proceed we must clarify two subtle points:

(a) Not all solutions with different τ_g are different. For example, it is easy to see that τ_g and $\tau_g \pm 1$ describe the same supergravity solution. The asymptotic torus of the supergravity solutions has a cycle that is special, namely the $(1,0)$ cycle (labeled by t) which is contractible in the interior. It is fairly easy to see that all inequivalent geometries can be characterized by specifying the cycle (p,q) of the gauge theory torus onto which the $(1,0)$ cycle of (7.9) is mapped when we conformally match the two tori. The two integers p and q have to be relatively prime.

JHEP01(2006)140

(*b*) We have to be careful about the boundary conditions of the fermions and the spin structures of the supergravity solutions. If there is a circle factor in the asymptotic geometry then we can choose either periodic or anti-periodic boundary conditions for the fermions along this circle if it is not contractible in the interior. However, if it is contractible then only anti-periodic boundary conditions are allowed. In our case the $(1,0)$ cycle of the gravity torus is contractible, so it has to be mapped to an anti-periodic cycle of the gauge torus. Since in our gauge theory analysis above we chose anti-periodic boundary conditions for the fermions on the $(1,0)$ and $(0,1)$ cycles of the gauge theory, we conclude that the acceptable geometries of (a) are those with $p+q$ odd.

Let us now analyze which solutions we have to include for a specific gauge theory on a torus with parameter τ whose partition function includes a contribution from (7.9). Up to a change of coordinates all these solutions should have the same asymptotics as (7.9), and they should involve identifications by some modular parameter τ' which is related by an $\mathrm{SL}(2,\mathbb{Z})$ transformation to τ. It is easy to verify that for this to be the case the parameters of the two metrics have to be related by $\widehat{\lambda}'\tau_2' = \widehat{\lambda}\tau_2$, and the u coordinates of the two metrics are related by $u'\sqrt{\tau_2'} = u\sqrt{\tau_2}$. Note that the relation between the $\widehat{\lambda}$'s is precisely the one we expect from the field theory point of view, for the two theories to have the coupling constant times area.

A straightforward computation of the (regularized) Euclidean action of the IIB solution (7.9) gives:

$$I = \frac{9N^2V_7}{64\widehat{\lambda}^2\pi^9}\tau_2\int_{u_0}^{R} du u^5, \tag{7.11}$$

where R is some very large radial position and V_7 is the volume of the unit 7-sphere. Using the results of the previous paragraph we see that if we compute $I(X_1) - I(X_2)$ for two solutions with τ and τ' related by a modular transformation, the divergent parts cancel and we find:

$$I(X_1) - I(X_2) = \frac{32N^2V_7}{9\sqrt{\widehat{\lambda}\tau_2}\pi^{3/2}}\left(-\tau_2^{3/2} + \tau_2'^{3/2}\right), \tag{7.12}$$

where we used $u_0^2 = \frac{16\pi^{5/2}}{3}\sqrt{\widehat{\lambda}}$. So, using the invariance of $\widehat{\lambda}\tau_2$, we conclude that the solution with the minimum action is the one which has the maximum value of τ_2 (and is consistent with $p+q = odd$).

Let us now see how this works in different regions of the τ_f plane. In regions I and II the geometry that dominates is $\tau_g = \tau_f$. It maps the $(1,0)$ cycle of the gravity torus to the $(1,0)$ cycle of the gauge torus. Any other solution with τ_g related by a modular transformation has a smaller τ_2 so it has a bigger action. Since the $(1,0)$ cycle is the only contractible cycle in the gravity solution, the Wilson loop around it will generically be nonzero $\langle \mathrm{tr}(U)\rangle \neq 0$, while all Wilson loops around any other cycle will be zero. Though it takes a little more work to see it, region IV is also dominated by the same geometry[15].

[15] In region IVa there is the geometry with the largest τ_2 is the $\tau_g = -\frac{1}{\tau_f - 1}$.However this would map the contractible $(1,0)$ cycle to $(1,\pm 1)$ which is a periodic cycle, so this is not an acceptable solution.

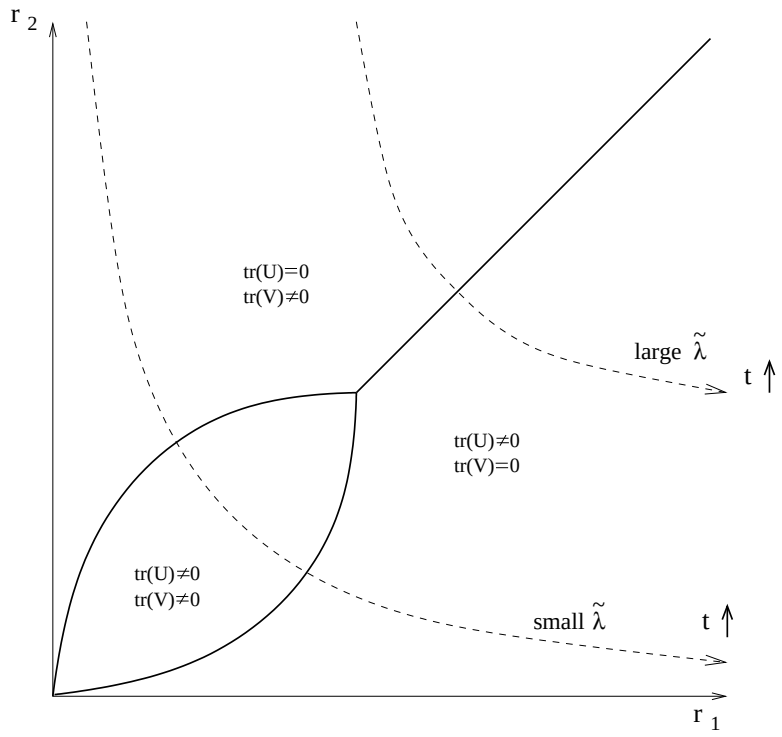

Figure 18: Conjectured phase diagram for SYM on a rectangular torus with anti-periodic boundary conditions on both cycles.

So, in summary, a single saddle point (7.8) dominates the thermodynamics of strongly coupled Yang-Mills theory on a torus in the fundamental region (the union of I, II, IV). The $(1,0)$ cycle is contractible on this solution, so $\langle \mathrm{tr}(V) \rangle = 0$ and $\langle \mathrm{tr}(U) \rangle \neq 0$ in this phase. For other regions we can find the dominant solution by mapping them into the fundamental region.

7.4 Putting it together

Let us summarize our understanding of the phase structure of this system. We begin by discussing tori with $\tau = it$ where t is real. At weak coupling the system is in the $\langle \mathrm{tr}(U) \rangle \neq 0$, $\langle \mathrm{tr}(V) \rangle = 0$ phase at large t. At $t = a/\sqrt{\tilde{\lambda}}$ the system undergoes a phase transition; at smaller values of t the system is in the $\langle \mathrm{tr}(U) \rangle \neq 0$, $\langle \mathrm{tr}(V) \rangle \neq 0$ phase. At $t = \sqrt{\tilde{\lambda}}/a$ the system undergoes another phase transition, to the $\langle \mathrm{tr}(U) \rangle = 0$, $\langle \mathrm{tr}(V) \rangle \neq 0$ phase. On the other hand, at strong coupling the analysis of the previous subsection shows that the system undergoes exactly one phase transition at $t = 1$. When $t > 1$, $\langle \mathrm{tr}(U) \rangle \neq 0$ and $\langle \mathrm{tr}(V) \rangle = 0$. On the other hand, when $t < 1$ $\langle \mathrm{tr}(V) \rangle \neq 0$ and $\langle \mathrm{tr}(U) \rangle = 0$. The phase diagram in figure 18 summarizes this behavior, and provides the simplest possible interpolation between these two limits.

Next, recall that a torus with $\mathrm{Re}(\tau) = 1$ may equally well be regarded as a rectangular torus with $\tau' = \tau - 1$ but with periodic boundary conditions along the τ axis. Following

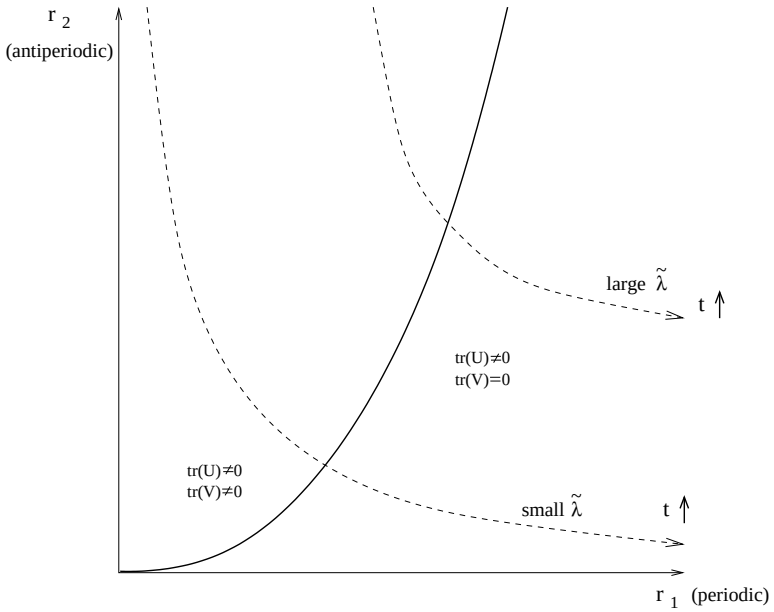

Figure 19: Phase diagram for SYM on a torus with one periodic and one anti-periodic boundary condition for the fermions. The large $\widetilde{\lambda}$ transition here is seen in the dual IIA description as a Gregory-Laflamme transition [3].

previous discussion in [3] we expect a phase transition associated only with the V holonomy, seen as a Gregory-Laflamme transition in the type IIA string description which is obtained by performing a T-duality on the periodic torus direction. Hence, we expect the phase diagram of figure 19 (or equivalently figure 1 in [3]). From the analysis in [3] we expect the phase transition to occur at $t \sim 1/\widetilde{\lambda}$ for large $\widetilde{\lambda}$. Note that this phase transition involves a new solution (localized in the T-dual direction) which is not included in the discussion of the previous subsection.

Using this information we conjecture the phase structure for a general value of τ. In figure 20 we show the two phase boundaries we expect for clumping of the V holonomies in the fundamental domain as a function of τ and $\widetilde{\lambda}$. For large $\widetilde{\lambda}$, the relevant boundary (shown in red) coincides with the boundary of the fundamental domain and corresponds also to anti-clumping of the U holonomy. For small $\widetilde{\lambda}$, the relevant boundary (shown in blue) involves only the transition of the V holonomy. As discussed earlier, modular transformations of this latter surface give other phase surfaces associated with transitions of different holonomies; for example, the clumping of the U holonomy is given by $\tau \to -1/\tau$. The $\mathrm{Re}(\tau) = 0$ slice reproduces the previous figure 18 when converting to r_1, r_2 coordinates and including this U transition. Likewise, the $\mathrm{Re}(\tau) = 1$ slice reproduces figure 19. Note that we expect that the two phase transition surfaces (red and blue) do not join smoothly for any $\mathrm{Re}(\tau)$, and their intersection moves to larger $\widetilde{\lambda}$ as we move nearer $\mathrm{Re}(\tau) = 1$, eventually leaving only the two phases with clumped U holonomy that are seen in [3].

By comparing figures 18 and 19 with the phase diagrams 13 and 14 of section 5, it is clear that for either choice of spatial boundary conditions, the supersymmetric theory

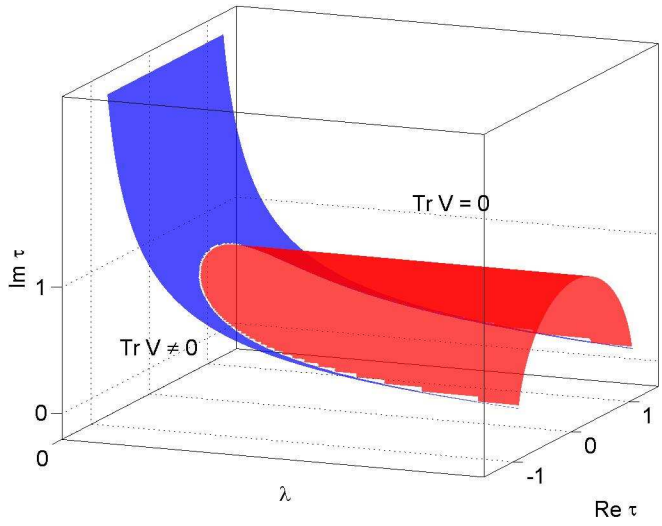

Figure 20: Conjectured phase boundaries for the V holonomy shown in the fundamental domain for general values of λ. The phase transition associated with the blue surface involves only the V holonomy, whilst the red surface corresponds also to a transition of the U holonomy.

has qualitatively different behavior from the bosonic theory. Curiously, the bosonic theory and the supersymmetric theory with anti-periodic-anti-periodic, anti-periodic-periodic, and periodic-periodic boundary conditions, have four, three, two, and one distinct phases, respectively.

Acknowledgments

We would like to thank Rajesh Gopakumar, Dan Jafferis, Subhaneil Lahiri, Andy Neitzke, Gordon Semenoff and Xi Yin for useful discussions. JM would like to thank IAS and KITP for hospitality during the course of this work. O.A., S.M., and K.P. would like to thank KITP for hospitality while this work was in progress. The work of O.A. was supported in part by the Israel-U.S. Binational Science Foundation, by the Israel Science Foundation (grant number 1399/04), by the Braun-Roger-Siegl foundation, by the European network HPRN-CT-2000-00122, by a grant from the G.I.F., the German-Israeli Foundation for Scientific Research and Development, and by Minerva. The work of J.M. was supported in part by an NSF Graduate Research Fellowship. The work of S.M. was supported in part by DOE grant DE-FG01-91ER40654, NSF career grant PHY-0239626, a Sloan fellowship, and a Harvard Junior Fellowship. The work of K.P. was supported in part by DOE grant DE-FG01-91ER40654. The work of M.V.R. has been supported in part by the Natural Sciences and Engineering Research Council of Canada and by the Canada Research Chairs Programme. T.W. is supported by NSF grant PHY-0244821.

JHEP01(2006)140

A. One-loop effective potentials for zero modes

In this appendix, we shall derive the one-loop effective action for the zero modes of SU(N) gauge theories with adjoint scalar fields in various dimensions, by integrating out all massive modes. We begin in appendix A.1 with an analysis of the effective action for the diagonal modes in the 0-dimensional matrix integral and its implications for the matrix integral discussed in section 3. The same analysis applies also to the KK zero modes of higher dimensional theories; in appendix A.2 we add the contribution of the higher KK modes as well, and in appendix A.3 we consider the one-loop contribution for supersymmetric Yang-Mills theories.

A.1 The zero mode integral

In this subsection we investigate the effective action for the matrix integral with p massless scalar fields discussed in section 3,

$$Z = \int \mathcal{D}\psi^\alpha \exp\left[-\frac{N}{4\lambda_0}\sum_{\alpha,\beta}\mathrm{tr}\left(\left[\psi^\alpha,\psi^\beta\right]^2\right)\right], \tag{A.1}$$

where $\alpha,\beta = 1,\cdots,p$. The same integral (except that some of the ψ^α's become periodic) arises for the zero modes of a d-dimensional gauge theory on T^d with p_d scalar fields and coupling constant λ_d; in this context $p = p_d + d$ since additional scalar fields arise from the gauge field, and λ_0 is λ_d divided by the volume of the T^d.

A naive extrapolation of the formula (3.4), giving the width of the eigenvalue distribution for large masses, to small masses would suggest that the eigenvalue distribution is infinitely spread out at $m = 0$. This estimate is too crude since it ignores the effect of the quartic restoring term in (A.1). Taking this term into account, a simple dimensional analysis suggests that the characteristic width scale for the eigenvalue distribution at the saddle point for $m = 0$ is given by $a = K\lambda_0^{\frac{1}{4}}$, where K is independent of N and λ_0. The N dependence of this estimate follows from 't Hooft scaling, while the λ_0-dependence is deduced from a simple change of variables in (A.1). However, this scaling argument cannot rule out the possibility that $K = \infty$, a danger that seems real given the fact that the quartic restoring term in (A.1) vanishes along a noncompact 'moduli space' along which all the matrices commute (and so may simultaneously be diagonalized). Consequently, the question of whether or not the eigenvalues in (A.1) clump at $m = 0$ is a dynamical issue [16]. One way to analyze this is by an analysis of the quantum effective action on the classical moduli space [27 – 29] that is obtained by integrating out the off diagonal modes. The generic effective mass of an off-diagonal mode is of order a, the width of the eigenvalue distribution. Consequently, as in the analysis of the massive theory in section 3, the effective coupling for the off diagonal modes is $\sim \lambda/a^4$; these modes may accurately be integrated out at one-loop provided that this coupling is small. This one-loop computation

[16] See [25] for a rigorous proof of the convergence of this integral, and [26] and references therein for a nice review and more details.

was performed in [28] and is reproduced, for the convenience of the reader, in the following paragraphs.

Let us expand around a configuration in which all matrices ψ^α are diagonal with eigenvalues ψ_i^α $(i = 1, \cdots, N)$, and integrate out the off-diagonal components of the matrices in (A.1) at 1-loop. Expanding the action (A.1) to quadratic order in the off-diagonal modes, we find

$$S^{\text{quadratic}}_{\text{zeromode}} = \frac{N}{4\lambda_0} \sum_{\alpha\neq\beta} \sum_{i<j} \left[(\Delta\psi^\alpha)^2_{ij}\, \psi^\beta_{ij}\psi^\beta_{ji} - (\Delta\psi^\alpha)_{ij} \left(\Delta\psi^\beta\right)_{ij} \psi^\alpha_{ij}\psi^\beta_{ji} \right], \tag{A.2}$$

where we defined $(\Delta\psi^\alpha)_{ij} = \psi^\alpha_i - \psi^\alpha_j$. Naively, integrating out the (ij)'th off-diagonal components of all the matrices simply yields $\det(M)^{-1}$, where M is the matrix

$$M^{\alpha\beta} = \delta^{\alpha\beta} \sum_\gamma (\Delta\psi^\gamma)^2_{ij} - (\Delta\psi^\alpha)_{ij}(\Delta\psi^\beta)_{ij}. \tag{A.3}$$

However, the eigenvalues of the matrix M are easily seen to be $[\sum_\gamma (\Delta\psi^\gamma)^2_{ij}]$ with degeneracy $p-1$ and zero with degeneracy one. The appearance of the zero eigenvalue is a result of the fact that we have neglected the existence of flat directions in the space of off-diagonal components, due to the remaining SU(N) gauge symmetry of (A.1), which can be used to rotate the diagonal components into off-diagonal components.

To correct for this, we eliminate these flat directions by using the SU(N) symmetry to diagonalize one of the ψ^α, say ψ^1, exactly. Performing this diagonalization by inserting a gauge-fixing δ-function introduces the Fadeev-Popov determinant factor

$$\det\left([\psi^1, *]\right) \sim \prod_{i\neq j} \left(\Delta\psi^1\right)_{ij} \sim \prod_{i<j} \left(\Delta\psi^1\right)^2_{ij}, \tag{A.4}$$

where we have evaluated the determinant at 1-loop.

Note that this factor is nothing more than the Vandermonde determinant appearing in the change of variables from the matrix ψ^1 to its eigenvalues.

Now there are no longer any off-diagonal components for ψ^1 in (A.2). This has the effect of removing the first row and column from the matrix M in (A.3). The eigenvalues of the resulting matrix are $[\sum_\gamma (\Delta\psi^\gamma)^2_{ij}]$ with degeneracy $p-2$ and $\left(\Delta\psi^1\right)^2_{ij}$ with degeneracy one. Having computed the relevant determinant, we may now write the contribution to the path integral from the gauge-fixing and from integrating out the off-diagonal components of the zero modes as

$$\frac{\prod_{i<j} \left(\Delta\psi^1\right)^2_{ij}}{\left[\prod_{i<j} (\Delta\psi^1)^2_{ij}\right] \left\{\prod_{i<j} \left[\sum_\gamma (\Delta\psi^\gamma)^2_{ij}\right]^{p-2}\right\}}. \tag{A.5}$$

The Fadeev-Popov factor in the numerator cancels the contribution from the eigenvalues depending only on ψ^1, leaving us with an expression which (as expected) is symmetric under permutations of the ψ^α's,

$$\prod_{i<j} \left[\sum_\gamma (\Delta\psi^\gamma)^2_{ij}\right]^{2-p}. \tag{A.6}$$

Thus, we find that the one-loop contribution to the matrix integral may be expressed as an integral over the eigenvalues of the matrices,

$$Z \propto \int \prod_{\alpha,i} d\psi_i^\alpha \frac{1}{\prod_{i<j} \left(\sum_\gamma (\psi_i^\gamma - \psi_j^\gamma)^2\right)^{(p-2)}} \quad \text{valid when } a^4 \gg \lambda_0. \tag{A.7}$$

In the large N limit it is natural to rewrite this in terms of an eigenvalue distribution function $\rho(\psi^\alpha)$, and to evaluate the integral by saddle points (since the action is proportional to N^2).

As all pairwise eigenvalue forces are attractive, the minimum of the action is attained when all eigenvalues sit at a point. Unfortunately this saddle point lies outside the domain of validity of (A.7), since it has $a = 0$. Thus, the one-loop analysis does not suffice to analyze the matrix integral, though it does reliably show that the eigenvalues attract each other at large distances. A more precise analysis shows that on the saddle point of (A.1) the eigenvalues have a sharply localized distribution with the scale $a \sim \lambda_0^{\frac{1}{4}}$, as suggested by the scaling arguments presented earlier in this section. This is verified by the Monte Carlo simulations shown in section 3, and was originally shown by similar methods in [29].

In summary, the behavior of (A.1) is qualitatively unaffected as the effective coupling constant λ_0/m^4 is varied from zero to infinity. The eigenvalue distribution of the matrix $\frac{1}{N}(\sum_\alpha (\psi^\alpha)^2)$ in (A.1) is governed by a saddle point that is always strictly localized; the localization length is given by $a^2 = \frac{p\lambda}{4m^2} f(\frac{\lambda}{m^4})$, where $f(0) = 1$ and $f(x) \propto 1/\sqrt{x}$ at large x.

A.2 Integrating out KK modes at 1-loop

We now consider a d-dimensional gauge theory compactified on a torus T^d with circles of circumference R_μ ($\mu = 1, \cdots, d$), and compute the effect of integrating out the KK modes at 1-loop on the effective action for the diagonal zero modes which we computed in the previous subsection. Consider the d-dimensional bosonic action[17]

$$S = \int d^d x \, \frac{N}{4\lambda} \, \mathrm{tr} \left[F_{\mu\nu} F_{\mu\nu} + \sum_I 2 D_\mu \phi^I D_\mu \phi^I - \sum_{I,J} \left[\phi^I, \phi^J\right]^2 \right], \tag{A.8}$$

with $p - d$ scalar fields, such that the zero mode action is given by (A.1), where ψ^μ ($\mu = 1, \cdots, d$) are the zero modes of A_μ, and ψ^{d+I} ($I = 1, \cdots, p-d$) are the zero modes of ϕ^I. We expand the fields A_μ, ϕ^I in KK modes $A_{\mu,\{m_\lambda\},ij}, \phi^I_{\{m_\lambda\},ij}$, with mode numbers $m_\lambda \in \mathbb{Z}$ around the λ'th circle. Expanding the action to quadratic order, we obtain

$$\begin{aligned} S = \frac{N}{4\lambda_0} \sum_{\{m^\mu\}} \sum_{i<j} \; & \left\{ \sum_\nu \left[\sum_{\mu \neq \nu} \left((\Delta\psi^\mu)_{ij} - \frac{2\pi m^\mu}{R_\mu} \right)^2 + \sum_I \left(\Delta\psi^{d+I} \right)^2_{ij} \right] |A_{\nu,\{m_\lambda\},ij}|^2 \right. \\ & \left. + \sum_I \left[\sum_\mu \left((\Delta\psi^\mu)_{ij} - \frac{2\pi m^\mu}{R_\mu} \right)^2 + \sum_{J \neq I} \left(\Delta\psi^{d+J} \right)^2_{ij} \right] |\phi^I_{\{m_\lambda\},ij}|^2 \end{aligned}$$

[17] If there are also fermionic fields, they decouple from the bosons at 1-loop so we can consider them separately as we will do below.

$$
\begin{aligned}
&-\sum_{\mu\neq\nu}\left((\Delta\psi^{\mu})_{ij}-\frac{2\pi m^{\mu}}{R_{\mu}}\right)\left((\Delta\psi^{\nu})_{ij}-\frac{2\pi m^{\nu}}{R_{\nu}}\right)A_{\mu,\{m_\lambda\},ij}A^{*}_{\nu,\{m_\lambda\},ij}\\
&-\sum_{I\neq J}\left(\Delta\psi^{d+I}\right)_{ij}\left(\Delta\psi^{d+J}\right)_{ij}\phi^{I}_{\{m_\lambda\},ij}\phi^{*,J}_{\{m_\lambda\},ij} \qquad (A.9)\\
&-\sum_{\mu,I}\left((\Delta\psi^{\mu})_{ij}-\frac{2\pi m^{\mu}}{R_{\mu}}\right)\left(\Delta\psi^{d+I}\right)_{ij}\left[A_{\mu,\{m_\lambda\},ij}\phi^{*,I}_{\{m_\lambda\},ij}+c.c.\right]\Bigg\}.
\end{aligned}
$$

Let us now perform a naive first attempt at integrating out the KK modes at one-loop. Defining a vector $D^{\alpha}_{ik,\{m_\lambda\}}$ as

$$
D_{ik,\{m_\lambda\}}=\left((\Delta\psi^{\mu})_{ik}-\frac{2\pi m_{\mu}}{R_{\mu}},\left(\Delta\psi^{d+I}\right)_{ik}\right)^{T}, \qquad (A.10)
$$

we see that performing the quadratic integral over KK modes in (A.9) yields a factor of $\det(M')^{-1}$, with

$$
M'=\left(D^{T}D\right)I-DD^{T}, \qquad (A.11)
$$

similar to what we found in the zero dimensional case. This determinant is easily evaluated, as the eigenvalues of M' are again D^TD with degeneracy $p-1$ and zero with degeneracy one. The appearance of a zero eigenvalue is not surprising. Indeed, it is expected as we have yet to fix the gauge. A convenient set of gauge-fixing constraints to adopt is the following:

$$
\begin{aligned}
\partial_1 A_1 &= 0,\\
\partial_2\int dx_1\,A_2 &= 0,\\
\partial_3\int dx_1\,dx_2\,A_3 &= 0,\\
&\cdots\\
\partial_d\int dx_1\ldots dx_{d-1}A_d &= 0. \qquad (A.12)
\end{aligned}
$$

For each constraint, we must also insert an appropriate Fadeev-Popov determinant factor. For the generic constraint

$$
\partial_{n+1}\int dx_1\,dx_2\ldots dx_n\,A_{n+1}=0, \qquad (A.13)
$$

the corresponding determinant takes the form

$$
\overset{(n)}{\det}\left(\partial_n\right)\overset{(n)'}{\det}\left(\partial_{n+1}-i\left[A_{n+1},*\right]\right), \qquad (A.14)
$$

where the superscript (n) is used to indicate that the determinant is taken over all modes of the gauge field that are constant in $x_1,\ldots,x_n$, while the prime in the second determinant indicates that it also includes only non-zero modes in x_{n+1}. We neglect the first, constant, determinant and evaluate the second one at one-loop, finding

$$
\prod_{i\neq j}\prod_{m^{\mu}}\left((\Delta\psi^{n+1})_{ij}-\frac{2\pi m^{n+1}}{R_{n+1}}\right)=\prod_{i<j}\prod_{m^{\mu}}\left((\Delta\psi^{n+1})_{ij}-\frac{2\pi m^{n+1}}{R_{n+1}}\right)^{2}, \qquad (A.15)
$$

where the product over m^μ is suitably constrained. Summarizing, we find that our gauge-fixing procedure introduces a factor of $\left((\Delta\psi^n)_{ij} - 2\pi m^n/R_n\right)^2$ for each mode of the gauge field which has $m^1 = \cdots = m^{n-1} = 0$ and $m^n \neq 0$.

Returning now to the task of integrating out the KK modes in (A.9), we write the gauge fixing constraints (A.12) as

$$\begin{aligned} A^1_{r,m_2,m_3,\ldots,m_d} &= 0 \\ A^2_{0,r,m_3,\ldots,m_d} &= 0 \\ &\cdots \\ A^d_{0,0,\ldots,0,r} &= 0, \end{aligned} \tag{A.16}$$

where $r \neq 0$ and the other m_μ are arbitrary. It is now easy to see that, for every choice of mode numbers $\{m_\lambda\}$, exactly one component of the gauge field, say $A_{\nu,\{m_\lambda\}}$, is eliminated by these constraints. When the corresponding row and column are removed from M', the eigenvalues become $D^T D$ with degeneracy $p-2$ and $\left((\Delta\psi^\nu)_{ij} - 2\pi m^\nu/R_\nu\right)^2$ with degeneracy one. Each factor of $\left((\Delta\psi^\nu)_{ij} - 2\pi m^\nu/R_\nu\right)^2$ that arises for a gauge field component eliminated by the gauge-fixing conditions, though, serves to cancel a corresponding factor from the Fadeev-Popov determinants (A.15), so that the final result obtained from gauge-fixing and integrating out KK modes at 1-loop is given by $\exp(-S_{eff,bos})$, where

$$S_{eff,bos} = (p-2)\sum_{\vec{m}\in\mathbb{Z}^d}\sum_{i<j}\ln\left[\sum_\mu\left((\Delta\psi^\mu)_{ij} - \frac{2\pi m^\mu}{R_\mu}\right)^2 + \sum_I\left(\Delta\psi^{d+I}\right)^2_{ij}\right]. \tag{A.17}$$

We have included also the terms (A.6) obtained from integrating out the off diagonal zero-modes. Like (A.7), the result corresponds to a pairwise logarithmic effective potential between the eigenvalues, but now these live on the dual torus in the gauge field directions, so we have additional interactions between the eigenvalues and the infinite set of image eigenvalues. These image interactions (corresponding to the sum over $\vec{m}$) ensure that the full result is periodic. This sum may be evaluated explicitly using the results of appendix B, and we find

$$\begin{aligned} S_{\text{eff, bos}} = &-2\left(\prod_\mu R_\mu\right)(p-2)\sum_{i<j}\theta_{ij}^{d/2}(2\pi)^{-d/2} \\ &\sum_{\vec{k}\in\mathbb{Z}^d-\{\vec{0}\}}\frac{1}{\left(\sum_\mu k_\mu^2 R_\mu^2\right)^{d/4}}e^{i\sum_\mu k_\mu R_\mu(\Delta\psi^\mu)_{ij}}K_{d/2}\left(\theta_{ij}\sqrt{\sum_\mu k_\mu^2 R_\mu^2}\right), \end{aligned} \tag{A.18}$$

where θ_{ij}^2 is defined as

$$\theta_{ij}^2 = \sum_I\left(\Delta\psi^{d+I}\right)^2_{ij}. \tag{A.19}$$

A.3 Generalization to supersymmetric field theories

It is a simple matter to include also fermionic fields, if they exist. Assuming that the Yukawa couplings to the scalars are the same as the gauge couplings, as in supersymmetric gauge theories, and that the fermions are periodic around $(d-1)$ of the circles but anti-periodic around the d'th circle, the appropriate determinant is easily computed and found to yield

$$\prod_{m^\nu}\prod_{i<j}\left[\sum_{\mu=1}^{d-1}\left((\Delta\psi^\mu)_{ij}-\frac{2\pi m^\mu}{R_\mu}\right)^2+\left(\left(\Delta\psi^d\right)_{ij}-\frac{2\pi(m^d+\frac{1}{2})}{R_d}\right)^2+\sum_I\left(\Delta\psi^{d+I}\right)_{ij}^2\right]^{p-2}. \tag{A.20}$$

As with (A.17), this corresponds to a pairwise potential between each eigenvalue and an infinite series of "images" of the remaining eigenvalues, except that the potential has the opposite sign and the coordinates of the images are shifted by a half period in any direction for which the fermions are anti-periodic.

Combining (A.6), (A.17), and (A.20), as appropriate for a supersymmetric gauge theory on a torus, we arrive at the full result:

$$Z=\int d\psi_i^\alpha\ \prod_{m^\nu}\prod_{i<j}\left[\frac{\sum_{\mu=1}^{d-1}\left((\Delta\psi^\mu)_{ij}-\frac{2\pi m^\mu}{R_\mu}\right)^2+\left(\left(\Delta\psi^d\right)_{ij}-\frac{2\pi(m^d+\frac{1}{2})}{R_d}\right)^2+\sum_I\left(\Delta\psi^{d+I}\right)_{ij}^2}{\sum_{\mu=1}^{d-1}\left((\Delta\psi^\mu)_{ij}-\frac{2\pi m^\mu}{R_\mu}\right)^2+\left((\Delta\psi^d)_{ij}-\frac{2\pi m^d}{R_d}\right)^2+\sum_I\left(\Delta\psi^{d+I}\right)_{ij}^2}\right]^{p-2}. \tag{A.21}$$

Using the results of appendix B we can again evaluate the product over mode numbers and obtain an effective action for the eigenvalue separations. The contribution from the fermionic sector is identical to the bosonic result (A.18), with the exception of an additional factor of $(-1)^{k_d+1}$ in the sum. As a result, the fermions serve to eliminate half of the terms in the k_d sum. Our final result for $S_{\rm eff}$ thus becomes:

$$\begin{aligned}S_{\rm eff}\ =\ &-4\left(\prod_\mu R_\mu\right)(p-2)\sum_{i<j}\theta_{ij}^{d/2}(2\pi)^{-d/2}\\ &\sum_{k_\mu=-\infty}^{\infty}\sum_{k_d\ odd}\frac{1}{\left(\sum_\mu k_\mu^2R_\mu^2\right)^{d/4}}e^{i\sum_\mu k_\mu R_\mu(\Delta\psi^\mu)_{ij}}K_{d/2}\left(\theta_{ij}\sqrt{\sum_\mu k_\mu^2R_\mu^2}\right).\end{aligned} \tag{A.22}$$

A.4 Analysis of the effective potentials for $d=2$

We will now focus on the case $d=2$, and argue that for both the bosonic and the supersymmetric cases, the eigenvalues of the gauge field will be clumped in all directions whenever the one-loop effective potentials (A.17) or (A.21) are reliable.

The contribution of the zero modes (corresponding to the $\vec{m}=0$ terms in the bosonic contribution to the potential) was discussed in appendix A.1, and we concluded that this leads the eigenvalues to clump at a scale

$$a\sim\lambda_0^{1/4}, \tag{A.23}$$

where $\lambda_0 = \lambda/(R_1 R_2)$. The additional terms in the effective potential correspond to the interactions with image eigenvalues. These interactions will be negligible for the clumped configuration as long as the scale (A.23) is much smaller than either $1/R_1$ or $1/R_2$ (i.e. when the distance to the nearest image charge is large compared with the distances between eigenvalues in the clump).[18] Since the KK-mode terms are important for configurations that are not highly clumped, we may worry that the full effective potentials (A.18) or (A.22) could have additional saddle point configurations. However, a quick analysis shows that in either case, the full effective potential (periodic in the directions corresponding to the gauge field eigenvalues) is attractive both for the scalar and for the gauge field zero modes,[19] so the eigenvalues are driven towards the clumped saddle point for which the KK-mode contributions are negligible. We conclude that the eigenvalues are clumped on a scale (A.23) whenever

$$\left(\frac{\lambda}{R_1 R_2}\right)^{\frac{1}{4}} \ll \frac{1}{R_1} \qquad \text{and} \qquad \left(\frac{\lambda}{R_1 R_2}\right)^{\frac{1}{4}} \ll \frac{1}{R_2}. \tag{A.24}$$

We see that the eigenvalues spread out relative to the sizes of the dual circles as either R_1 or R_2 increases, suggesting a possible phase transition when either of the inequalities in (A.24) is violated. However, the effective coupling of the lightest KK-modes is λ_0/m_{KK}^4, so when the relations (A.24) are not satisfied, either the R_1 or the R_2 KK-modes become strongly coupled and we can no longer trust our perturbative results for the effective potential. Therefore, other methods (discussed in the main text) are required to deduce the presence (or not) of a phase transition as the eigenvalues spread.

A.5 Integrating out massive scalars

Before closing this section, we describe the result of integrating out a set of p very massive adjoint scalar fields in a two dimensional gauge theory on T^2. In general, the one-loop result is given by (5.18), where D_μ is the covariant derivative for the adjoint representation. Here, we consider the special case where the gauge fields are constant commuting matrices, so that the holonomies are $U = e^{iR_2 A_2}$ and $V = e^{iR_1 A_1}$. Then

$$\begin{aligned} S_{\text{eff}} &= \frac{p}{2} \ln(\det(-D_\mu^2 + M^2)) \\ &= \frac{p}{2} \operatorname{tr}(\ln(-D_1^2 - D_2^2 + M^2)) \\ &= \frac{p}{2} \operatorname{tr}\left(\sum_{m,n} \ln\left(\left(\frac{2\pi n}{R_1} + A_1\right)^2 + \left(\frac{2\pi m}{R_2} + A_2\right)^2 + M^2\right)\right) \end{aligned}$$

[18] It is not immediately obvious that the infinite set of image charges does not conspire to produce a larger effect, but because of cancellations between $\vec{m}$ and $-\vec{m}$ terms in the potential, it may be checked that the sum of contributions from all charges is of the same order of magnitude as the contribution from the nearest charge.

[19] There is one qualitative difference between the bosonic and supersymmetric cases. In the supersymmetric case, the potential between two eigenvalues actually goes to infinity as the eigenvalues approach antipodal points in the anti-periodic directions, since in this configuration there is a (repulsive) image charge from one eigenvalue sitting on top of the other eigenvalue.

$$= -\frac{p}{2\pi} M R_1 R_2 \sum_{k,l} \mathrm{tr}(U^l V^k)\, \mathrm{tr}(U^{-l} V^{-k}) \frac{K_1(M\sqrt{(kR_1)^2 + (lR_2)^2})}{\sqrt{(kR_1)^2 + (lR_2)^2}} \tag{A.25}$$

where in the last line, we have used a result from appendix B.

B. Infinite products

In evaluating the determinants involved in integrating out Kaluza-Klein modes and massive scalars in the main text and in appendix A, we encounter infinite products whose logarithm gives an infinite sum of the form

$$P(\vec{a}) = \sum_{\vec{m}} \ln(\theta^2 + (\vec{m} + \vec{a})^2). \tag{B.1}$$

Here, the sum runs over all vectors $\vec{m}$ in d dimensions with integer components. Now, P is clearly periodic in each component of $\vec{a}$, with period 1. Thus, we can write

$$P(\vec{a}) = \sum_{\vec{k}} e^{2\pi i \vec{k}\cdot\vec{a}} P_{\vec{k}}, \tag{B.2}$$

and we can compute the Fourier transform of P:

$$\begin{aligned}
P_{\vec{k}} &= \int_0^1 da_1 \cdots \int_0^1 da_d \sum_{\vec{m}} \ln(\theta^2 + (\vec{m} + \vec{a})^2)\; e^{-2\pi i \vec{k}\cdot\vec{a}} \\
&= \sum_{\vec{m}} \int_{m_1}^{m_1+1} da_1 \cdots \int_{m_d}^{m_d+1} da_d\; \ln(\theta^2 + \vec{a}^2)\; e^{-2\pi i \vec{k}\cdot\vec{a}} \\
&= \int d\vec{a}\; \ln(\theta^2 + \vec{a}^2)\; e^{-2\pi i \vec{k}\cdot\vec{a}} \\
&= lim_{\epsilon\to 0} \left(-\ln(\epsilon) - \int_\epsilon^\infty \frac{d\alpha}{\alpha} e^{-\alpha\theta^2} \int d\vec{a}\; e^{-\alpha\vec{a}^2 - 2\pi i \vec{k}\cdot\vec{a}} \right) \\
&= C_\infty - \pi^{\frac{d}{2}} \int_0^\infty \frac{d\alpha}{\alpha^{\frac{d}{2}+1}} e^{-\alpha\theta^2 - \frac{\pi^2 k^2}{\alpha}} \\
&= C_\infty - 2\frac{\theta^{\frac{d}{2}}}{|\vec{k}|^{\frac{d}{2}}} K_{\frac{d}{2}}(2\pi|\vec{k}|\theta).
\end{aligned} \tag{B.3}$$

Here, C_∞ is an infinite constant independent of k and θ.

C. Effective action for the Wilson line in $d = 1$ gauge theories

In this appendix, we consider the one dimensional Euclidean gauge theory on a circle of circumference R with p scalars and action

$$S = \int dt\, \mathrm{tr} \left(\frac{1}{2} D_t \Phi_i D_t \Phi_i + \frac{M}{2} \Phi_i \Phi_i - \frac{g^2}{4} [\Phi_i, \Phi_j][\Phi_i, \Phi_j] \right). \tag{C.1}$$

The analysis here follows that of [30], which considered the special case of two scalar fields. Note that here we have rescaled the gauge field and the scalar fields by a factor of g

compared to our previous analysis, so as to have canonical kinetic terms. We would like to integrate out the scalar fields for small values of the dimensionless 't Hooft coupling g^2N/M^3, to obtain an effective action in terms of the Wilson line of the gauge field around the circle. We choose the gauge $\partial_t A_0 = 0$, so that A_0 is a t-independent Hermitian matrix $A_0 = \alpha$. With this choice, the Wilson line is simply given by

$$U = e^{i\alpha R} \ . \tag{C.2}$$

We define

$$\exp(-S_{\rm eff}(U)) = \int [d\Phi_i] e^{-S(\Phi,\alpha)}, \tag{C.3}$$

in terms of which the partition function is given by

$$Z = \int DU \exp(-S_{\rm eff}(U)) \ . \tag{C.4}$$

As explained in section 4 of [2], the Haar measure DU arises from the initial measure $[dA_0]$ upon introducing the Fadeev-Popov determinant associated with the gauge fixing condition $\partial_t A_0 = 0$.

By gauge invariance, the effective action must be some function of the variables

$$u_n \equiv \frac{1}{N} \mathrm{tr}(U^n) \ . \tag{C.5}$$

At one-loop order, the calculation of $S_{\rm eff}$ was described in [2], with the result

$$S_{\rm eff}^{1-loop}(U) = N^2 \sum_{n=1}^{\infty} \frac{1}{n}(1 - px^n)|u_n|^2, \tag{C.6}$$

where $x = e^{-RM}$. Here, the x-independent term is a rewriting of the Vandermonde determinant obtained in writing the Haar measure in terms of eigenvalues. For $x < 1/p$, the one-loop effective action is positive definite, minimized by the saddle-point configuration $u_n = 0$. As x passes $x_c = 1/p$, the mode u_1 becomes unstable and condenses to its maximum allowed value (as long as all other $u_n = 0$) $u_1 = 1/2$, giving rise to a first order large N phase transition in the strict $g^2N = 0$ limit.

As described in section 6 of [2], in order to determine the nature of the phase transition for weak but non-zero coupling, it is necessary to take into account higher order terms in the effective action. The relevant physics may be deduced easily from the effective action for u_1, obtained by integrating out both the scalar fields and all the modes $u_{n>1}$ near the transition. This takes the general form

$$S_{\rm eff}(u_1) = N^2(m_1^2(x,\lambda)|u_1|^2 + b(x,\lambda)|u_1|^4 + \mathcal{O}(\lambda^4)) \ , \tag{C.7}$$

where in perturbation theory b starts at order λ^2. If the coefficient b is positive at the value x_c of x where m_1^2 drops to zero, we will have a second order phase transition with the eigenvalue distribution for U changing continuously. On the other hand if (as we will find below) the coefficient b is negative at this value $x = x_c$, the potential develops a

second minimum which is lower than the first already at some slightly lower value of x, the eigenvalue distribution changes discontinuously, and we have a first order phase transition.

The leading order contribution to b is given by

$$b = D_3 - \frac{C_2^2}{B_1}, \tag{C.8}$$

where B_1, C_2, and D_3 are the leading coefficients of the terms $|u_2|^2$, $(u_2 u_{-1}^2 + u_{-2} u_1^2)$, and $|u_1|^4$ in the effective action obtained by integrating out the scalars; these terms first arise at one, two, and three-loop order, respectively. We now proceed to compute these coefficients, together with the corrections to the coefficient $A = N^2 m_1^2$ of $|u_1|^2$, needed to determine how the phase transition temperature varies with the coupling constant.

The higher loop corrections to the effective action are given by

$$S_{\text{eff}}^{pert} = \langle -e^{-\frac{g^2}{4}\operatorname{tr}([\Phi^i,\Phi^j]^2)} \rangle_{\text{connected}}. \tag{C.9}$$

This may be evaluated in perturbation theory using the propagator

$$\langle (\Phi_i)_{kl}(t_1)(\Phi_j)_{mn}(t_2) \rangle = \Delta_{kn}(t_1 - t_2, \alpha)\delta_{lm} - \delta_{kn}\Delta_{lm}(t_1 - t_2, \alpha), \tag{C.10}$$

where the matrix Δ is defined by

$$\Delta(t, \alpha) = \frac{e^{i\alpha t}}{2M}\left(\frac{e^{-tM}}{1 - e^{-M\beta} e^{i\alpha R}} - \frac{e^{tM}}{1 - e^{M\beta} e^{i\alpha R}} \right). \tag{C.11}$$

More details about the perturbative evaluation and our conventions may be found in [15]. Setting $M = 1$ for now, the contribution to the effective action from the two-loop figure eight diagram is given by

$$S_{\text{eff}}^{2\ loop} = \frac{g^2}{2}\beta(p^2 - p)\operatorname{tr}(\Delta(0, \alpha_{ab})\Delta(0, \alpha_{ac}))\ , \tag{C.12}$$

where we have introduced the notation $\alpha_{ab} = \alpha_a - \alpha_b$, with

$$\alpha_a = \alpha \otimes 1 \otimes 1, \qquad \alpha_b = 1 \otimes \alpha \otimes 1, \qquad \alpha_c = 1 \otimes 1 \otimes \alpha. \tag{C.13}$$

This leads to quadratic terms

$$S_{\text{quad}}^{2\ \text{loop}} = -\frac{1}{4}N^2\lambda(p^2 - p)\ln(x)\sum_n (x^{2n} + 2x^n)|u_n|^2, \tag{C.14}$$

and leading order cubic terms

$$S_{\text{cubic}}^{2\ \text{loop}} = -\frac{1}{8}N^2\lambda(p^2 - p)\ln(x)(x^2 + 2x^3)(u_2 u_{-1}^2 + u_{-2}u_1^2) + \dots\ . \tag{C.15}$$

At three loops, the diagrams 3a, 3b, and 3c shown in figure 21 give the following contributions

$$\begin{aligned}
S_{\text{eff}}^{3a} &= -\frac{1}{2}g^4(p^2 - p)\beta \int dt \operatorname{tr}(\Delta(t, \alpha_{ab})\Delta(t, \alpha_{bc})\Delta(t, \alpha_{cd})\Delta(t, \alpha_{da})), \\
S_{\text{eff}}^{3b} &= -\frac{1}{2}g^4 p(p-1)^2\beta \int dt \operatorname{tr}(\Delta(0, \alpha_{ab})\Delta(t, \alpha_{ac})\Delta(t, \alpha_{ca})\Delta(0, \alpha_{ad})), \\
S_{\text{eff}}^{3c} &= -\frac{1}{2}g^4 p(p-1)^2\beta \int dt \operatorname{tr}(\Delta(0, \alpha_{ab})\Delta(t, \alpha_{ac})\Delta(t, \alpha_{ca})\Delta(0, \alpha_{cd})).
\end{aligned} \tag{C.16}$$

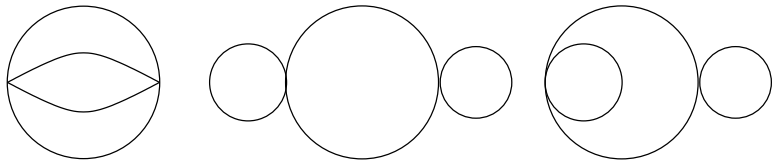

Figure 21: Three-loop diagrams contributing to the effective action.

These contribute to the quadratic term for the lowest mode

$$\begin{aligned}
S^{3a}_{\text{quad}} &= -\frac{1}{16}N^2\lambda^2|u_1|^2(p^2-p)\ln(x)x(2x\ln(x)+x^2-x-3),\\
S^{3b}_{\text{quad}} &= -\frac{1}{16}N^2\lambda^2|u_1|^2p(p-1)^2\ln(x)x(\ln(x)(2x+1)-3(x+1)),\\
S^{3c}_{\text{quad}} &= -\frac{1}{16}N^2\lambda^2|u_1|^2p(p-1)^2\ln(x)x(\ln(x)(x+1)^2-(x^2+2x+3)).
\end{aligned} \tag{C.17}$$

The same diagrams also give the leading $|\operatorname{tr}(U)|^4$ terms,

$$\begin{aligned}
S^{3a}_{\text{quart}} &= -\frac{1}{32}N^2\lambda^2|u_1|^4(p^2-p)\ln(x)x^2(2\ln(x)+2x^2-5),\\
S^{3b}_{\text{quart}} &= -\frac{3}{16}N^2\lambda^2|u_1|^4p(p-1)^2\ln(x)x^3(\ln(x)-1),\\
S^{3c}_{\text{quart}} &= -\frac{1}{16}N^2\lambda^2|u_1|^4p(p-1)^2\ln(x)x^2(2x^2\ln(x)-x^2-2).
\end{aligned} \tag{C.18}$$

Collecting our results, we have

$$S_{\text{eff}} = A|u_1|^2 + B_1|u_2|^2 + C_2(u_2u_{-1}^2 + u_{-2}u_1^2) + D_3|u_1|^4 + \dots \tag{C.19}$$

where

$$\begin{aligned}
A/N^2 &= (1-px) - \frac{1}{4}\lambda(p^2-p)\ln(x)(x^2+2x)\\
&\quad -\frac{1}{16}\lambda^2(p^2-p)x\ln(x)(2x\ln(x)+x^2-x-3)\\
&\quad -\frac{1}{16}\lambda^2p(p-1)^2x\ln(x)(\ln(x)(x^2+4x+2)-x^2-5x-6)+\mathcal{O}(\lambda^3),\\
B_1/N^2 &= \frac{1}{2}(1-px^2)+\mathcal{O}(\lambda),\\
C_2/N^2 &= -\frac{1}{8}\lambda(p^2-p)\ln(x)(x^2+2x^3)+\mathcal{O}(\lambda^2),\\
D_3/N^2 &= -\frac{1}{32}\lambda^2(p^2-p)\ln(x)x^2(2\ln(x)+2x^2-5)\\
&\quad -\frac{1}{16}\lambda^2p(p-1)^2\ln(x)x^2(\ln(x)(2x^2+3x)-x^2-3x-2)+\mathcal{O}(\lambda^3).
\end{aligned} \tag{C.20}$$

From these above expressions and from (C.8) we find that

$$b(x=x_c=1/p)/N^2 = -\frac{1}{32}\frac{(p-1)\ln(p)}{p^3}(\ln(p)(9p^2+2p)+4p^3+7p^2-4p-4)\lambda^2, \tag{C.21}$$

which is negative for all $p > 1$. Thus, the phase transition is of first order at weak coupling.

To determine the precise transition point as a function of λ, we note that to order λ^2, the second minimum $|u_1| = 1/2$ will become dominant at the point x_c where

$$m_1^2(x)\frac{1}{2^2} + b(x)\frac{1}{2^4} = 0. \tag{C.22}$$

Solving perturbatively for x_c as a function of λ, we find

$$\begin{aligned} x_c = &\frac{1}{p} + \lambda\frac{(p-1)(2p+1)\ln(p)}{4p^2} \\ &+\lambda^2\frac{(p-1)\ln(p)}{128p^4}((16p^4-33p^2-10p)\ln(p) - 80p^4 - 20p^3 + 41p^2 + 28p + 4) + \mathcal{O}(\lambda^3). \end{aligned} \tag{C.23}$$

Expressing this as an equation for $\widetilde{t} = 1/(R\lambda^{1/3})$ as a function of $m = M/\lambda^{1/3}$ gives the relation (4.6) .

D. Pure and deformed Yang-Mills partition functions on T^2

In this appendix, we review the exact solution of pure Yang-Mills theory on T^2 [9], and use techniques developed by Gross and Taylor [31 – 33] in order to write the result at large N in terms of an effective action for one of the two holonomies, U and V. We then proceed to study the partition function for a class of deformations which are encountered in section 5.

D.1 Pure Yang-Mills theory on T^2

An exact expression for the partition function of pure Yang-Mills theory on T^2 is easily obtained, following Migdal [9], if we use a particular lattice regularization of the theory. We put unitary matrices U_L on the links on the lattice, and consider the partition function

$$Z = \int \prod_L dU_L \prod_P Z_P(U_P), \tag{D.1}$$

where P denotes the plaquettes of the lattice, U_P is a product of the U_L's around the plaquette P, and Z_P is a plaquette action chosen so that the continuum theory coincides with Yang-Mills theory (for instance, the Wilson action $Z_P = \exp(\frac{1}{g_{YM}^2}\operatorname{tr}(U_P + U_P^{-1}))$).

Migdal noted that, upon integrating out various links, one is left with an action of the form (D.1) with a plaquette action for the remaining (larger) plaquettes that approaches a weighted sum of characters χ_R, in the representation R of the gauge group:

$$Z_P(U_P) = \sum_R d_R\chi_R(U_P)e^{-\frac{\lambda A}{2N}C_2(R)}, \tag{D.2}$$

where the representation R has dimension d_R and quadratic Casimir $C_2(R)$, λ is the dimensionless 't Hooft coupling, and A is the area of the plaquette[20]. Using standard orthogonality relations, it is easy to verify the additivity property of (D.2),

$$\int DU\, Z_P(V_1U, \lambda A_1)Z_{P'}(U^\dagger V_2, \lambda A_2) = Z_{P+P'}(V_1V_2, \lambda(A_1 + A_2)), \tag{D.3}$$

[20] In [9], Migdal considered a more general situation in which (D.1) was not required to yield pure Yang-Mills theory in the continuum limit. As such, he originally wrote the factor in the exponent in terms of a representation-dependent coupling, g_R, noting that $g_R^2 \to g_{YM}^2 C_2(R)$ gives the correct Coulomb law. One can also see this directly by applying Migdal's analysis to the Wilson action.

JHEP01(2006)140

at which point (D.1) can be reduced to an integral over two matrices, U and V, corresponding to the products of the U_L's over the links along the two non-trivial cycles of the torus:

$$Z_{ym} = \int DU\, DV \sum_R d_R e^{-\frac{\widetilde{\lambda}}{2N} C_2(R)} \chi_R(UVU^{-1}V^{-1}) \,, \tag{D.4}$$

where $\widetilde{\lambda}$ is the 't Hooft coupling times the area of the T^2. We can then use the result

$$\int DU\, \chi_R(UAU^{-1}B) = \frac{1}{d_R}\chi_R(A)\chi_R(B) \tag{D.5}$$

to integrate out one matrix, say U, from (D.4), obtaining

$$Z_{ym} = \int DV \sum_R e^{-\frac{\widetilde{\lambda}}{2N} C_2(R)} \chi_{R\otimes\bar{R}}(V). \tag{D.6}$$

This integral is also trivial to perform, since $R \otimes \bar{R}$ contains the identity precisely once, yielding the well-known expression for Z_{ym} purely as a function of $\widetilde{\lambda}$,

$$Z_{ym} = \sum_R e^{-\frac{\widetilde{\lambda}}{2N} C_2(R)}. \tag{D.7}$$

In the rest of this subsection, we shall be interested in determining, in the limit of large N, a more explicit form for the effective action, $S_{\text{eff}}(V)$, corresponding to the partition function (D.6).

Thus, we seek a large N expansion of the quadratic Casimir and character appearing there. As pointed out by Gross and Taylor in [31]-[33], one may obtain the correct large N expansion of (D.6) by summing independently over representations formed from tensor products of finitely many fundamentals and anti-fundamentals. The Young tableaux for any such representation may be obtained uniquely by adjoining the Young tableau for some representation obtained from the product of finitely many anti-fundamentals with the Young tableau for some representation obtained from the product of finitely many fundamentals. Following the notation in [31, 33] we denote these representations by $\bar{S}$ and R respectively, and denote the representation corresponding to the original tableau, termed the "composite" representation of R and S, by $T = \bar{S}R$.

Letting n_R (n_S) denote the number of boxes associated to the representation R (S), we may express the quadratic Casimir of the composite representation T in terms of those of its components as:

$$C_2(T) = C_2(R) + C_2(S) + \frac{2n_R n_S}{N^2}, \tag{D.8}$$

where

$$C_2(R) = Nn_R + \mathcal{O}(N^0) \,, \qquad C_2(S) = Nn_S + \mathcal{O}(N^0) \,. \tag{D.9}$$

Denoting the set of Young tableaux with n boxes by T_n, and denoting both an arbitrary element of T_n and the representation corresponding to it by $Y_n \in T_n$, we may now write (D.6) at large N as

$$Z_{ym} = \int DV \sum_{n,n'} \sum_{Y_n \in T_n} \sum_{Y'_{n'} \in T_{n'}} e^{-(n+n')\frac{\widetilde{\lambda}}{2}} \chi_{(\bar{Y}'_{n'} Y_n)\otimes(\overline{\bar{Y}_n Y'_{n'}})}(V). \tag{D.10}$$

We now seek to expand the characters appearing in the integrand as a polynomial in traces. To proceed, we first define some further notation. To any given tableau, $Y_n \in T_n$, we may associate not only an irreducible representation, also denoted by Y_n, of SU(N), but also an irreducible representation, $\widehat{Y}_n$, of the permutation group S_n. We use $\chi_{Y_n}(V)$ to denote the character of the SU(N) representation Y_n evaluated on $V \in \mathrm{SU}(N)$, and $\chi_{\widehat{Y}_n}(\sigma)$ to denote the character of the S_n representation $\widehat{Y}_n$ evaluated on $\sigma \in S_n$. To each tableau, $Y_n \in T_n$, we also associate a conjugacy class, ρ_{Y_n}, of S_n, which can also be labeled by the numbers $\{\sigma_i\}$, which specify the number of cycles of length i in an element of ρ_{Y_n}. Finally, we let Υ_σ denote the Schur function associated to $\sigma \in S_n$,

$$\Upsilon_\sigma(V) = \sum_{Y_n \in T_n} \chi_{\widehat{Y}_n}(\sigma)\chi_{Y_n}(V) = \prod_i \mathrm{tr}(V^i)^{\sigma_i}. \tag{D.11}$$

The character of any representation $Y_n \in T_n$ is easily expanded in terms of Schur functions

$$\chi_{Y_n}(V) = \frac{1}{n!}\sum_{\sigma \in S_n} \chi_{\widehat{Y}_n}(\sigma)\Upsilon_\sigma(V). \tag{D.12}$$

To study (D.6), we shall need the following generalized version of (D.12) for composite representations that was worked out by Gross and Taylor [33]:

$$\chi_{\bar{Y}'_{n'}Y_n}(V) = \frac{1}{n!n'!}\sum_{\sigma \in S_n}\sum_{\tau \in S_{n'}} \chi_{\widehat{Y}_n}(\sigma)\chi_{\widehat{Y}'_{n'}}(\tau)\Upsilon_{\bar{\tau}\sigma}(V, V^\dagger), \tag{D.13}$$

where

$$\begin{aligned}
\Upsilon_{\bar{\tau}\sigma}(V, V^\dagger) &= \sum_{Y_n \in T_n}\sum_{Y'_{n'} \in T_{n'}} \chi_{\widehat{Y}_n}(\sigma)\chi_{\widehat{Y}'_{n'}}(\tau)\chi_{\bar{Y}'_{n'}Y_n}(V) \\
&= \prod_l \Upsilon_{\bar{\tau}^{(l)}\sigma^{(l)}}(V, V^\dagger), \\
\Upsilon_{\bar{\tau}^{(l)}\sigma^{(l)}}(V, V^\dagger) &= \sum_{k=0}^{\min(\sigma_l,\tau_l)} \binom{\sigma_l}{k}\binom{\tau_l}{k}(-1)^k l^k k!\,\mathrm{tr}(V^l)^{\sigma_l - k}\,\mathrm{tr}(V^{-l})^{\tau_l - k}.
\end{aligned} \tag{D.14}$$

Using this result, we may now write (D.6) as

$$\begin{aligned}
Z_{ym} = \int DV \sum_{n,n'}\sum_{\sigma,\sigma' \in S_n}\sum_{\tau,\tau' \in S_{n'}}\sum_{Y_n \in T_n}\sum_{Y'_{n'} \in T_{n'}} e^{-(n+n')\frac{\tilde{\lambda}}{2}} \times \\
\frac{\chi_{\widehat{Y}_n}(\sigma)\chi_{\widehat{Y}_n}(\sigma')\chi_{\widehat{Y}'_{n'}}(\tau)\chi_{\widehat{Y}'_{n'}}(\tau')}{(n!)^2(n'!)^2} \times \Upsilon_{\bar{\tau}\sigma}(V, V^\dagger)\Upsilon_{\bar{\sigma}'\tau'}(V, V^\dagger).
\end{aligned} \tag{D.15}$$

The sum over Young tableaux can be performed using the completeness relation

$$\frac{1}{n!}\sum_{Y_n \in T_n} \chi_{\widehat{Y}_n}(\sigma)\chi_{\widehat{Y}_n}(\sigma') = \frac{1}{|\rho_\sigma|}\delta_{\rho_\sigma,\rho_{\sigma'}}, \tag{D.16}$$

where ρ_σ denotes the conjugacy class to which σ belongs and $|\rho_\sigma|$ its dimension. Using this result we obtain

$$\begin{aligned} Z_{ym} &= \int DV \sum_{n,n'} \sum_{\sigma\in S_n} \sum_{\tau\in S_{n'}} \frac{e^{-\frac{\widetilde{\lambda}}{2}(n+n')}}{n!n'!} \Upsilon_{\bar{\tau}\sigma}(V,V^\dagger)\Upsilon_{\bar{\sigma}\tau}(V,V^\dagger) \\ &= \int DV \sum_{n,n'} \sum_{\sigma\in S_n} \sum_{\tau\in S_{n'}} \frac{e^{-\frac{\widetilde{\lambda}}{2}(n+n')}}{n!n'!} \prod_l \{ \Big[\mathrm{tr}(V^l)\,\mathrm{tr}(V^{-l})\Big]^{\sigma_l+\tau_l} \times \\ &\quad \sum_{k,k'=0}^{\min(\sigma_l,\tau_l)} \binom{\sigma_l}{k}\binom{\sigma_l}{k'}\binom{\tau_l}{k}\binom{\tau_l}{k'} (-l)^{k+k'} k!k'! \Big[\mathrm{tr}(V^l)\,\mathrm{tr}(V^{-l})\Big]^{-(k+k')} \}. \end{aligned} \tag{D.17}$$

We now replace the sums over σ,τ with (appropriately weighted) sums over the σ_i,τ_j which label conjugacy classes. Typically, such sums must be subject to the restrictions $\sum_i i\sigma_i = n$, $\sum_j j\tau_j = n'$ and are difficult to evaluate. Fortunately, the sums over n,n' serve to lift these restrictions, leaving us with the following expression

$$\begin{aligned} Z_{ym} = \int DV \prod_l \Bigg\{ &\sum_{\sigma_l,\tau_l=0}^{\infty} \sum_{k,k'=0}^{\min(\sigma_l,\tau_l)} \left(\frac{e^{-\frac{\widetilde{\lambda}l}{2}}}{l}\right)^{\sigma_l+\tau_l} \Big[\mathrm{tr}(V^l)\,\mathrm{tr}(V^{-l})\Big]^{\sigma_l+\tau_l} \\ &\times \frac{\sigma_l!\tau_l!}{k!k'!(\sigma_l-k)!(\sigma_l-k')!(\tau_l-k)!(\tau_l-k')!} (-l)^{k+k'} \Big[\mathrm{tr}(V^l)\,\mathrm{tr}(V^{-l})\Big]^{-(k+k')} \Bigg\}, \end{aligned} \tag{D.18}$$

which can be rewritten as

$$\begin{aligned} Z_{ym} = \int DV \prod_l \Bigg\{ &\sum_{\sigma,\tau=0}^{\infty} \sum_{k,k'=0}^{\infty} \left(\frac{e^{-\frac{\widetilde{\lambda}l}{2}}}{l}\right)^{\sigma+\tau+2\max(k,k')} \frac{(-l)^{k+k'}}{\sigma!\tau!k!k'!} \\ &\times \left[\frac{[\sigma+\max(k,k')]!\,[\tau+\max(k,k')]!}{[\sigma+|k-k'|]!\,[\tau+|k-k'|]!}\right] \Big[\mathrm{tr}(V^l)\,\mathrm{tr}(V^{-l})\Big]^{\sigma+\tau+|k-k'|} \Bigg\}. \end{aligned} \tag{D.19}$$

We now consider the sum at fixed l, which may be rewritten, after a little algebra, as

$$\begin{aligned} &\sum_{\sigma,\tau,k'=0}^{\infty} \sum_{k=-\infty}^{\infty} \frac{1}{\sigma!\tau!k'!} \left(\frac{e^{-\frac{\widetilde{\lambda}l}{2}}}{l}\right)^{\sigma+\tau} \left(-\frac{e^{-\widetilde{\lambda}l}}{l}\right)^{|k|} \left(e^{-\widetilde{\lambda}l}\right)^{k'} \left[\frac{(\sigma+|k|+k')!(\tau+|k|+k')!}{(\sigma+|k|)!(\tau+|k|)!(|k|+k')!}\right] \\ &\qquad \times \Big[\mathrm{tr}(V^l)\,\mathrm{tr}(V^{-l})\Big]^{\sigma+\tau+|k|}. \end{aligned} \tag{D.20}$$

In our large N limit, (D.20) becomes

$$\exp\left[\left(\frac{2e^{-\frac{\widetilde{\lambda}l}{2}} - e^{-\widetilde{\lambda}l}}{l}\right)\mathrm{tr}(V^l)\,\mathrm{tr}(V^{-l})\right], \tag{D.21}$$

with corrections that are subleading in N in the exponent. As a result we find that (D.17) can be written as

$$Z_{ym} = \int DV\, \exp\Big\{-S_{\mathrm{eff}}(V,\widetilde{\lambda})\Big\}, \tag{D.22}$$

where

$$S_{\rm eff}(V,\widetilde{\lambda}) = \sum_{l=1}^{\infty}\left[\left(e^{-\frac{\widetilde{\lambda}l}{2}}-1\right)^2-1\right]\left(\frac{{\rm tr}(V^l)\,{\rm tr}(V^{-l})}{l}\right). \tag{D.23}$$

To study this result, we write it in terms of the moments $u_n \equiv {\rm tr}(V^n)/N$ of the eigenvalue distribution,

$$Z_{ym} \sim \int (\prod_n d^2u_n)\,\exp\left\{-N^2\sum_{n=1}^{\infty}\frac{\left(e^{-\frac{n\widetilde{\lambda}}{2}}-1\right)^2}{n}|u_n|^2\right\}. \tag{D.24}$$

A model similar to this was studied in [2]. Here, the masses of all moments, u_n, are positive for all positive values of the coupling, $\widetilde{\lambda}$, and thus the dominant eigenvalue distribution is the uniform one with $u_n = 0$ for all nonzero n. At large N, the u_n are essentially independent variables and can be integrated out to yield

$$Z_{ym} \sim \prod_n \left(1-e^{-\frac{\widetilde{\lambda}n}{2}}\right)^{-2}. \tag{D.25}$$

This is in agreement with the known partition function for pure Yang-Mills theory on T^2 at large N.

D.2 Deformed Yang-Mills theory on T^2

In this appendix, we derive a formula relevant to our study in section 5 of pure Yang-Mills theory deformed by very massive scalars. In section 5.5, we argue that in a certain regime of parameter space, integrating out very massive adjoint scalars gives, to a good approximation, an expression (5.24) for the partition function, where f and g depend only on the eigenvalues of U and V respectively. Now, changing variables $U \to WUW^{-1}$ and integrating over W (which doesn't change the result since the integrand cannot depend on W) we obtain

$$Z_{ym} = \int DW\,DU\,DV\,\sum_R d_R e^{-\frac{\widetilde{\lambda}}{2N}C_2(R)}\chi_R(WUW^{-1}VWU^{-1}W^{-1}V^{-1})e^{-f(U)}e^{-g(V)}. \tag{D.26}$$

Here, we have used the invariance of both the measure DU and of the function $f(U)$ under the transformation used in the change of variables. To proceed further, we seek to evaluate the integral

$$I(D_1,D_2) = \int DC\,\chi_R(CD_1C^{-1}D_2CD_1^{-1}C^{-1}D_2^{-1}). \tag{D.27}$$

Using SU(N) symmetry, the form of $I(D_1,D_2)$ is restricted to

$$\begin{aligned} I(D_1,D_2) = {}& \alpha + \beta\left[\chi_R(D_1)\chi_R(D_1^{-1}) + \chi_R(D_2)\chi_R(D_2^{-1})\right] \\ & +\gamma\chi_R(D_1)\chi_R(D_1^{-1})\chi_R(D_2)\chi_R(D_2^{-1}). \end{aligned} \tag{D.28}$$

To compute $I(D_1,D_2)$, we thus need only to determine the three numbers α,β,γ. To constrain their values, let us first look at $I(1,D_2)$. Equating (D.27) and (D.28) we obtain

$$\alpha + \beta\left[d_R^2 + \chi_R(D_2)\chi_R(D_2^{-1})\right] + \gamma d_R^2\chi_R(D_2)\chi_R(D_2^{-1}) = d_R. \tag{D.29}$$

We next consider integrating $\int DD_1 I(D_1, D_2)$. Comparing the result obtained by interchanging the integrations over D_1 and C yields

$$\alpha + \beta \left[1 + \chi_R(D_2)\chi_R(D_2^{-1})\right] + \gamma\chi_R(D_2)\chi_R(D_2^{-1}) = \frac{1}{d_R}\chi_R(D_2)\chi_R(D_2^{-1}). \tag{D.30}$$

Equations (D.29) and (D.30) give 4 equations relating the coefficients α, β, γ:

$$\begin{aligned} \alpha + \beta d_R^2 &= d_R, \\ \beta + \gamma d_R^2 &= 0, \\ \alpha + \beta &= 0, \\ \beta + \gamma &= \frac{1}{d_R}. \end{aligned} \tag{D.31}$$

This system has a unique solution

$$\begin{aligned} \alpha &= -\frac{d_R}{d_R^2 - 1}, \\ \beta &= \frac{d_R}{d_R^2 - 1}, \\ \gamma &= -\frac{1}{d_R(d_R^2 - 1)}. \end{aligned} \tag{D.32}$$

Applying (D.28) with these values to our expression (D.26), we may rewrite Z_{YM} as (5.25).

E. More about the Monte-Carlo simulations

The Monte-Carlo simulations presented here were written using an elementary implementation of the Metropolis algorithm. The ensembles were fully thermalized between samplings with various time-time correlators being checked.

In the case of the 0+0 matrix integrals the implementation is extremely simple. For the 0+1 matrix quantum mechanics we require a lattice of L spatial sites, with circle topology, and each site is equipped with the scalar adjoint matter matrices, with the gauge field living as usual on the links. Since the gauge dynamics is trivial in this low dimension we may perform a gauge transformation to make the unitary link variables equal on all sites. Furthermore we may use up the remaining gauge freedom by diagonalizing this unitary link matrix. The remaining diagonal components are pure phases, and are physical, giving the eigenvalues of the Polyakov loop when raised to the power L, the number of lattice sites. We carefully ensure that the Jacobian introduced by this gauge fixing is properly implemented. This unitary matrix measure is the non-perturbative version of the Vandermonde determinant and is given by $\Pi_{i<j} \sin^2 \frac{L}{2}(\theta_i - \theta_j)$ for $i = 1, \cdots, N$, where $e^{i\theta_i}$ are the eigenvalues of the unitary link. This measure factor is implemented by taking its log and introducing it as a potential term in the action. We automatically adjust the Metropolis step size to ensure decent acceptance rates, and use independent step sizes for the unitary link eigenvalues, and for both the scalar adjoint matter diagonal, and off-diagonal components.

JHEP01(2006)140

For the large N behaviour we study we require relatively few lattice points to accurately capture the continuum behaviour. For p scalars with $p = 2, 4$ the data presented here uses 10 lattice points. For the $p = 9$ data 5 lattice sites were used. For individual values of λ and M we checked that this was sufficient for the quantities we measured, finding that doubling or quadrupling the number of lattice sites did not change the results at the level of one percent.

References

[1] B. Sundborg, *The hagedorn transition, deconfinement and $N = 4$ sym theory*, *Nucl. Phys.* **B 573** (2000) 349 [hep-th/9908001].

[2] O. Aharony, J. Marsano, S. Minwalla, K. Papadodimas and M. Van Raamsdonk, *The hagedorn/deconfinement phase transition in weakly coupled large-N gauge theories*, *Adv. Theor. Math. Phys.* **8** (2004) 603 [hep-th/0310285].

[3] O. Aharony, J. Marsano, S. Minwalla and T. Wiseman, *Black hole - black string phase transitions in thermal 1+1 dimensional supersymmetric Yang-Mills theory on a circle*, *Class. and Quant. Grav.* **21** (2004) 5169 [hep-th/0406210].

[4] L. Susskind, *Matrix theory black holes and the gross Witten transition*, hep-th/9805115.

[5] M. Li, E.J. Martinec and V. Sahakian, *Black holes and the SYM phase diagram*, *Phys. Rev.* **D 59** (1999) 044035 [hep-th/9809061].

[6] E.J. Martinec and V. Sahakian, *Black holes and the SYM phase diagram, II*, *Phys. Rev.* **D 59** (1999) 124005 [hep-th/9810224].

[7] G. 't Hooft, *A planar diagram theory for strong interactions*, *Nucl. Phys.* **B 72** (1974) 461.

[8] K. Demeterfi, I.R. Klebanov and G. Bhanot, *Glueball spectrum in a (1+1)-dimensional model for QCD*, *Nucl. Phys.* **B 418** (1994) 15 [hep-th/9311015].

[9] A.A. Migdal, *Recursion equations in gauge field theories*, *Sov. Phys. JETP* **42** (1975) 413.

[10] B.E. Rusakov, *Loop averages and partition functions in* U(N) *gauge theory on two-dimensional manifolds*, *Mod. Phys. Lett.* **A 5** (1990) 693.

[11] E. Witten, *On quantum gauge theories in two-dimensions*, *Commun. Math. Phys.* **141** (1991) 153.

[12] D.S. Fine, *Quantum Yang-Mills on the two-sphere*, *Commun. Math. Phys.* **134** (1990) 273.

[13] M. Blau and G. Thompson, *Quantum Yang-Mills theory on arbitrary surfaces*, *Int. J. Mod. Phys.* **A 7** (1992) 3781.

[14] G.W. Semenoff, O. Tirkkonen and K. Zarembo, *Exact solution of the one-dimensional non-abelian Coulomb gas at large-N*, *Phys. Rev. Lett.* **77** (1996) 2174 [hep-th/9605172].

[15] O. Aharony, J. Marsano, S. Minwalla, K. Papadodimas and M. Van Raamsdonk, *A first order deconfinement transition in large-N Yang-Mills theory on a small S^3*, *Phys. Rev.* **D 71** (2005) 125018 [hep-th/0502149].

[16] E. Witten, *Constraints on supersymmetry breaking*, *Nucl. Phys.* **B 202** (1982) 253.

[17] T. Banks, W. Fischler, S.H. Shenker and L. Susskind, *M-theory as a matrix model: a conjecture*, *Phys. Rev.* **D 55** (1997) 5112 [hep-th/9610043].

JHEP01(2006)140

[18] J.M. Maldacena, *The large-N limit of superconformal field theories and supergravity*, *Adv. Theor. Math. Phys.* **2** (1998) 231 [hep-th/9711200].

[19] N. Itzhaki, J.M. Maldacena, J. Sonnenschein and S. Yankielowicz, *Supergravity and the large-N limit of theories with sixteen supercharges*, *Phys. Rev.* **D 58** (1998) 046004 [hep-th/9802042].

[20] J.M. Maldacena, *Wilson loops in large-N field theories*, *Phys. Rev. Lett.* **80** (1998) 4859 [hep-th/9803002].

[21] S.-J. Rey and J.-T. Yee, *Macroscopic strings as heavy quarks in large-N gauge theory and anti-de Sitter supergravity*, *Eur. Phys. J.* **C 22** (2001) 379 [hep-th/9803001].

[22] E. Witten, *Anti-de Sitter space, thermal phase transition and confinement in gauge theories*, *Adv. Theor. Math. Phys.* **2** (1998) 505 [hep-th/9803131].

[23] J.M. Maldacena and A. Strominger, *AdS_3 black holes and a stringy exclusion principle*, *JHEP* **12** (1998) 005 [hep-th/9804085].

[24] R. Dijkgraaf, J.M. Maldacena, G.W. Moore and E.P. Verlinde, *A black hole Farey tail*, hep-th/0005003.

[25] P. Austing and J.F. Wheater, *Convergent Yang-Mills matrix theories*, *JHEP* **04** (2001) 019 [hep-th/0103159].

[26] P. Austing, *Yang-Mills matrix theory*, hep-th/0108128.

[27] H. Aoki, S. Iso, H. Kawai, Y. Kitazawa and T. Tada, *Space-time structures from IIB matrix model*, *Prog. Theor. Phys.* **99** (1998) 713 [hep-th/9802085].

[28] T. Hotta, J. Nishimura and A. Tsuchiya, *Dynamical aspects of large-N reduced models*, *Nucl. Phys.* **B 545** (1999) 543 [hep-th/9811220].

[29] W. Krauth and M. Staudacher, *Eigenvalue distributions in Yang-Mills integrals*, *Phys. Lett.* **B 453** (1999) 253 [hep-th/9902113].

[30] J. Leyland-Harris, *Analysis of phase transitions in weakly coupled large N gauge theories in 0+1 dimensions*, UBC Undergraduate Thesis, April 2004.

[31] D.J. Gross, *Two-dimensional QCD as a string theory*, *Nucl. Phys.* **B 400** (1993) 161 [hep-th/9212149].

[32] D.J. Gross and W. Taylor, *Two-dimensional QCD is a string theory*, *Nucl. Phys.* **B 400** (1993) 181 [hep-th/9301068].

[33] D.J. Gross and W. Taylor, *Twists and Wilson loops in the string theory of two-dimensional QCD*, *Nucl. Phys.* **B 403** (1993) 395 [hep-th/9303046].

JHEP01(2006)140